

A Comprehensive Discussion of HSQC and HMQC Pulse Sequences

PRAVAT K. MANDAL,¹ ANANYA MAJUMDAR²

¹ *Neurophysics Laboratory, Department of Psychiatry, University of Pittsburgh Medical Center, Pittsburgh, Pennsylvania 15213*

² *Memorial Sloan-Kettering Cancer Center, 1275 York Avenue, New York, New York 10021*

ABSTRACT: Much of the progress in NMR applications over the last decade has stemmed from the development of proton-detected, heteronuclear multidimensional spectroscopy. The basic building blocks of the multitude of double and triple resonance experiments available today are the heteronuclear multiple quantum correlation (HMQC) and heteronuclear single quantum correlation (HSQC) experiments. The goal of this article is to provide a comprehensive, pedagogical description of these two pulse sequences, with the aid of product operator formalism. Building from basic principles, constant-time experiments, sensitivity-enhanced techniques and the role of pulsed-field gradients for coherence transfer pathway selection are explained in detail. This article is intended to be used as a primer for students and researchers seeking a firm theoretical understanding of the fundamental tools of modern NMR pulse sequences. © 2004 Wiley Periodicals, Inc. Concepts Magn Reson Part A 20A: 1–23, 2004

KEY WORDS: Cartesian product operators; polarization transfer; INEPT; HMQC; HSQC; pulsed field gradients; sensitivity improvement; constant-time evolution

INTRODUCTION

NMR spectroscopy has experienced several revolutionary upheavals in the last 25 years or so, especially in the field of biomolecular NMR. First, the introduction of homonuclear, two-dimensional (2D) tech-

niques (1–5) rendered biomolecules as large as 10 kD amenable to NMR studies. In the last decade, with the rapid development of isotopic labeling techniques, proton-detected heteronuclear NMR spectroscopy has allowed even larger molecules to be studied by NMR. Modern NMR techniques consist of a seemingly endless multitude of pulse sequences and remains in a state of continuous evolution. However, two simple building blocks are the root of these experiments, the heteronuclear single quantum coherence (HSQC) and heteronuclear double quantum coherence (HMQC) experiments. A clear understanding of more complicated multidimensional experiments requires a clear understanding of the HSQC and HMQC modules. In this article, we present a detailed description of these

Received 16 May 2003; revised 22 August 2003; accepted 26 August 2003

Correspondence to: Pravat K. Mandal; E-mail: mandalp@upmc.edu

This article is dedicated to Professor Jay W. Pettegrew.

Concepts in Magnetic Resonance Part A, Vol. 20A(1) 1–23 (2004)

Published online in Wiley InterScience (www.interscience.wiley.com). DOI 10.1002/cmra.10095

© 2004 Wiley Periodicals, Inc.

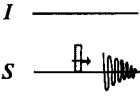
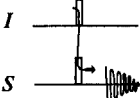
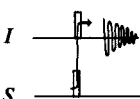
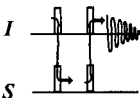
	Type of transfer	Relative sensitivity	S = ^{13}C	S = ^{15}N
(A)		$\gamma_S^{5/2}$	1	1
(B)		$\gamma_I \gamma_S^{3/2}$	4	10
(C)		$\gamma_I^{3/2} \gamma_S$	8	30
(D)		$\gamma_I^{5/2}$	32	300

Figure 1 Relative sensitivities of various heteronuclear coherence transfer experiments. Here, I -spin corresponds to proton and sensitivities are relative to direct observation of the S -spin (7).

two basic modules: Often, a seemingly complex 3D, triple resonance experiment is simply a concatenation of several HSQC and/or HMQC steps. The material presented here should be a useful learning aid for students and researchers familiar with the basics of product operator formalism and who are eager to absorb the intricacies of more complex experiments.

All multidimensional heteronuclear NMR experiments correlate one or more heteronuclear nuclei (usually labeled S , Q , etc.) with a protein (I) resonance through appropriate coherence transfer steps (6–9). The overall sensitivity (S/N) of a heteronuclear correlation experiment (7) is proportional to

$$S/N \propto \gamma_{\text{ex}} \gamma_{\text{det}}^{3/2} [1 - \exp(-R_{1,\text{ex}} T_C)] \quad [1]$$

where γ_{ex} and γ_{det} are the gyromagnetic ratios of the nucleus excited at the beginning and detected at the end of the sequence, respectively; T_C is the recycle time of the experiment; and $R_{1,\text{ex}}$ is the spin-lattice relaxation rate constant of the excited nucleus.

Several options for designing heteronuclear experiments are shown in Fig. 1. From a sensitivity point of view, it is highly advantageous to excite the proton, followed by polarization transfer to the heteronucleus, and subsequently reverse polarization transfer to the proton for detection [Fig. 1(D)]. Müller (10) first developed such a pulse sequence for heteronuclear correlation. This pulse sequence was later popularized

by Bax et al. (11) and is presently known as heteronuclear double quantum coherence (HMQC). Subsequently, heteronuclear single quantum coherence (HSQC) sequence was developed (12). The distinction between these two proton-detected heteronuclear correlation techniques (10–14) is that IS -spin coherence is stored as multi-quantum (HMQC) or single-quantum (HSQC), during the t_1 evolution period.

BUILDING BLOCKS

The easiest way to understand complex NMR experiments is to identify the building blocks from which these experiments are constructed with the help of product operator formalism (15). The “right-hand rule” for rotations is assumed, which is consistent with the treatment proposed by Sørensen et al. (15) but opposite to that of Van de Ven and Hilbers (16–18). Before describing these experiments, however, it is worthwhile to review the basic features of multiple pulse experiments.

Refocusing

Refocusing pulses play an important part in multiple-phase NMR experiments. A perfect refocusing pulse changes the sign of a given coherence, $p \rightarrow -p$. Refocusing of chemical shifts and the heteronuclear scalar couplings can be achieved by a spin-echo period: a 180° pulse placed in the center of a free precession period (18–20). Figure 2(A) illustrates a situation where both chemical shift as well as heteronuclear spin-spin coupling are refocused. Two distinct situations may arise.

Case A(i). Transverse I -spin magnetization evolves simultaneously under the influence of chemical shift and spin-spin coupling. However, if the two Hamiltonians, chemical shift (\mathcal{H}_{CS}) ($\mathcal{H}_{\text{CS}} = \Omega_I I_Z + \Omega_S S_Z$) and spin-spin (\mathcal{H}_{SS}) ($\mathcal{H}_{\text{SS}} = 2\pi J_{IS} I_Z S_Z$) contain commuting parts (see Appendix, Scheme I), then these two effects can be examined independently of each other. A product operator analysis of the effect of chemical shift evolution on I_Y , between points (a–d) in [Fig. 2(A)], is given below.

$$(a \rightarrow b) \quad -I_Y \xrightarrow{(\Omega_I \tau) I_Z} -I_Y \cos \Omega_I \tau + I_X \sin \Omega_I \tau$$

$$(b \rightarrow c) \quad \xrightarrow{(180^\circ) I_Y} -I_Y \cos \Omega_I \tau - I_X \sin \Omega_I \tau$$

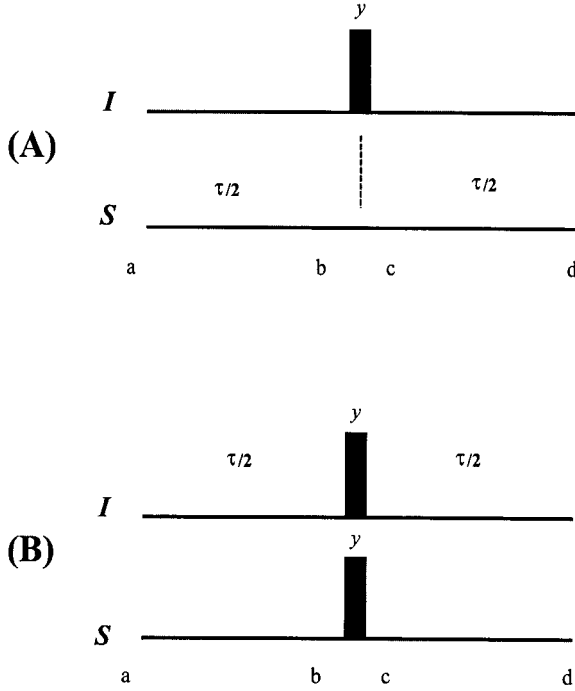


Figure 2 Variation of spin-echo building blocks. (A) The effect of selective 180° pulse on chemical shift as well as heteronuclear spin-spin coupling, J_{IS} . (B) The effect of nonselective 180° pulse on chemical shift as well as heteronuclear spin-spin coupling J_{IS} . Magnetization at different points (a–d) is described in the text. Thin and dark vertical bars refer to 90° and 180° pulses, respectively.

$$(c \rightarrow d) \xrightarrow{(\Omega_I \tau) I_z} -I_Y \cos^2 \Omega_I \tau + I_X \sin \Omega_I \tau \cos \Omega_I \tau - I_X \sin \Omega_I \tau \cos \Omega_I \tau - I_Y \sin^2 \Omega_I \tau = -I_Y \quad [2a]$$

So, at the end of the 2τ precession period the state of the system returns to $-I_Y$ (i.e., refocused). Now we consider the effect of case of IS scalar coupling during evolution alone, the same analysis [between a and d, Fig. 2(A)] yields

$$\begin{aligned} (a \rightarrow b) & \xrightarrow{2J_{IS}I_ZS_Z} -I_Y \cos(\pi J_{IS}\tau/2) \\ & \quad + 2I_X S_Z \sin(\pi J_{IS}\tau/2) \\ (b \rightarrow c) & \xrightarrow{(180^\circ)I_Y} -I_Y \cos(\pi J_{IS}\tau/2) \\ & \quad - 2I_X S_Z \sin(\pi J_{IS}\tau/2) \\ (c \rightarrow d) & \xrightarrow{2J_{IS}I_ZS_Z} -I_Y \cos^2(\pi J_{IS}\tau/2) \\ & \quad + 2I_X S_Z \sin(\pi J_{IS}\tau/2) \cos(\pi J_{IS}\tau/2) \end{aligned}$$

$$\begin{aligned} & - 2I_X S_Z \sin(\pi J_{IS}\tau/2) \cos(\pi J_{IS}\tau/2) \\ & - I_Y \sin^2(\pi J_{IS}\tau/2) = -I_Y \quad [2b] \end{aligned}$$

Thus, an equal interval $\tau/2$ before and after the application of 180° pulse on the I -spin refocuses its chemical shift as well as heteronuclear scalar couplings.

Case A(ii). In this case, the evolution of transverse $-S_Y$ magnetization will be considered. First, consider evolution due to chemical shift alone:

$$\begin{aligned} (a \rightarrow b) & \xrightarrow{(\Omega_S \tau/2) S_Z} -S_Y \cos \Omega_S \tau/2 + S_X \sin \Omega_S \tau/2 \\ (b \rightarrow c) & \xrightarrow{(180^\circ)I_Y} -S_Y \cos \Omega_S \tau/2 + S_X \sin \Omega_S \tau/2 \\ (c \rightarrow d) & \xrightarrow{(\Omega_S \tau/2) S_Z} -S_Y \cos^2 \Omega_S \tau/2 \\ & \quad + S_X \sin \Omega_S \tau \cos \Omega_S \tau/2 + S_X \sin \Omega_S \tau/2 \cos \Omega_S \tau/2 \\ & \quad + S_Y \sin^2 \Omega_S \tau/2 = -S_Y \cos \Omega_S \tau + S_X \sin \Omega_S \tau \quad [2c] \end{aligned}$$

We find, not surprisingly, that application of an 180° pulse on spin I does not affect the chemical shift evolution of spin S , since $H_{CS}(S) = \Omega_S S_Z$. However, the spin-spin coupling, which is proportional to $I_z S_z$, is refocused, as show below:

$$\begin{aligned} (a \rightarrow b) & \xrightarrow{2J_{IS}I_ZS_Z} -S_Y \cos(\pi J_{IS}\tau/2) + 2S_X I_Z \sin(\pi J_{IS}\tau/2) \\ (b \rightarrow c) & \xrightarrow{(180^\circ)I_Y} -S_Y \cos(\pi J_{IS}\tau/2) - 2S_X I_Z \sin(\pi J_{IS}\tau/2) \\ (c \rightarrow d) & \xrightarrow{2J_{IS}I_ZS_Z} -S_Y \cos^2(\pi J_{IS}\tau/2) + 2S_X I_Z \sin(\pi J_{IS}\tau) \cos(\pi J_{IS}\tau/2) \\ & \quad - 2S_X I_Z \sin(\pi J_{IS}\tau/2) \cos(\pi J_{IS}\tau) \\ & \quad - S_Y \sin^2(\pi J_{IS}\tau/2) = -S_Y \quad [2d] \end{aligned}$$

We arrive at the following conclusions regarding an IS spin pair in which at least one of the nuclei is transverse:

- The application of a 180° pulse on the transverse nucleus refocuses its chemical shift as well as scalar coupling evolution over a period of time symmetrically distributed about the 180° pulse.

If the sequence is asymmetric, i.e., $\tau_1 - 180^I - \tau_2$, both chemical shift and scalar couplings are refocused for a period $(\tau_1 - \tau_2)$.

- The application of a 180° pulse on the nontransverse nucleus, over the same period of time, effectively decouples the scalar coupling between the two spins, but does not affect the chemical shift evolution of the transverse nucleus.

Case B. Unlike the earlier case, two 180° (Y) pulses are applied simultaneously to both I - and S -spins [Fig. 2(B)]. The fate of $-I_Y$ due to scalar coupling evolution at different points (a–d) is shown below:

$$\begin{aligned}
 (a \rightarrow b) & \xrightarrow{2J_{IS}I_ZS_Z} -I_Y \cos(\pi J_{IS}\tau/2) + 2I_XS_Z\sin(\pi J_{IS}\tau/2) \\
 (b \rightarrow c) & \xrightarrow{(180^\circ)(I_Y + S_Y)} -I_Y \cos(\pi J_{IS}\tau/2) + 2I_XS_Z\sin(\pi J_{IS}\tau/2) \\
 (c \rightarrow d) & \xrightarrow{2J_{IS}I_ZS_Z} -I_Y \cos^2(\pi J_{IS}\tau/2) \\
 & + 2I_XS_Z\sin(\pi J_{IS}\tau)\cos(\pi J_{IS}\tau/2) \\
 & + 2I_XS_Z\sin(\pi J_{IS}\tau/2)\cos(\pi J_{IS}\tau) + I_Y\sin^2(\pi J_{IS}\tau/2) \\
 & = -I_Y \cos(\pi J_{IS}\tau) + 2I_XS_Z\sin(\pi J_{IS}\tau) \quad [2e]
 \end{aligned}$$

We therefore conclude:

- Application of simultaneous 180° pulses on both nuclei over a symmetric $\tau - (180^I, 180^S) - \tau$ period, refocuses chemical shift of the transverse nucleus and retains evolution under the J -coupling over the entire 2τ period.
- For an asymmetric sequence $\tau_1 - (180^I, 180^S) - \tau_2$, chemical shifts are refocused over a period $(\tau_1 - \tau_2)$, whereas couplings evolve over a period $(\tau_1 + \tau_2)$.

Coherence Transfer Pathways

Coherence is a generalization of the idea of transverse magnetization in NMR. Transverse magnetization corresponds to a coherence order of $p = \pm 1$ and is associated with product operators such as $I_{X,Y}$, $2I_ZS_{X,Y}$, etc. in which only one nucleus is associated with “transverse” operators (“ xy ”), whereas all others are either “ z ” or identity. Higher orders of coherences are represented by product operators consisting of multiple transverse operators. For example, an oper-

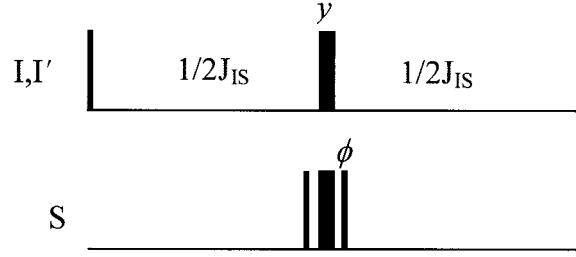


Figure 3 Spin-echo difference experiment illustrating basic phase-cycling principles. Narrow and broad pulses represent 90° and 180° pulses, respectively, with phase x , unless specified explicitly. If the phase $\phi = x$, I and S are decoupled, and both I' and I spin magnetization refocus with the same phase at the end of the sequence. If $\phi = -x$, the IS coupling remains active over a period $1/J_{IS}$ and therefore, I and I' magnetizations refocus with opposite phase. Addition or subtraction of two FIDs acquired with the phase ϕ cycled x , $-x$ yields pure I -spin or pure I' -spin spectra.

ator such as $2I_XS_Y$ may be decomposed into a sum and difference of double- and zero-quantum operators. For spin- $\frac{1}{2}$ nuclei, the highest coherence order possible is equal to the total number of coupled spins. A detailed discussion of coherence order pathways can be found in Ernst et al. (7) and Bain (21). The aim of any given pulse sequence is to selectively retain a specific coherence transfer pathway and eliminate all others. Selection of a desired coherence pathway is achieved either by phase cycling or the use of pulsed field gradients. Both approaches are described with simple examples.

Coherence Pathway Selection

Phase Cycles. For a given pulse sequence consisting of multiple pulses and delays, more than one coherence transfer pathway exists. The term phase cycling refers to the process of repeating a pulse sequence with a systematic variation of the relative phase of the pulses within the sequence to retain a specific coherence transfer pathway. A formal treatment of phase cycling concepts and methodologies is beyond the scope of this review and can be found elsewhere (21, 22). However, a simple example relevant to heteronuclear experiments called the spin-echo difference sequence is presented here. Consider an ensemble of spins consisting of coupled I - S spin pairs and uncoupled I' spins in a natural abundance study of ^{13}C -bound proton sample consisting of 1% ^{13}C - and 99% ^{12}C -bound protons, respectively. If we wish to obtain a 1D spectrum consisting of ^{13}C -bound protons only, we can use the pulse sequence shown in Fig. 3.

Beginning from an initial state of $(-I_y - I'_y)$, we follow the fate of the I and I' spins over a spin-echo period $1/J_{IS}$. Because the I' spins are not coupled to S , they are not affected by pulses on the S spin and, therefore, are always refocused with the same phase. The fate of these I spins, however, depends on the net effect of the 90_x° – 180_x° – 90_ϕ° sequence of pulses on S , based on whether the phase ϕ of the $90^\circ(S)$ pulse is x or $-x$. If $\phi = x$, the total flip angle associated with the 90_x° – 180_x° – 90_x° sequence is $360^\circ \equiv 0^\circ$ and therefore, the net effect is that of no pulse being applied on S . In that case, I_y behaves identically to I'_y , i.e., refocuses with the same phase. On the other hand, if $\phi = -x$, the net flip angle of the 90_x° – 180_x° – $90_{(-x)}^\circ$ sequence is 180_x° on S , and, therefore, the J_{IS} coupling remains active throughout the $1/J_{IS}$ period. The total evolution under the scalar coupling is given by

$$\begin{aligned} -I_y &\xrightarrow{J_{IS}} -I_y \cos(\pi J_{IS} t) + 2I_x S_z \sin(\pi J_{IS} t) \\ &= -I_y(-1) = I_y \quad \text{for } t = 1/J_{IS} \quad [2f] \end{aligned}$$

Because of the coupling evolution, the phase of I spins invert relative to I' (which, of course, is inert with respect to changes in ϕ). As a result, if we record two FIDs, with a phase-cycle $\phi = x, -x$ and subtract them (often denoted by the concomitant cycling of the receiver phase $\phi_R = x, -x$), only the I -spin spectrum remains, whereas the I' signals are canceled. By the same token, if we wish to purge I -spin spectrum and retain only the I' spins, we would add the two FIDs ($\phi = x, -x$; $\phi_R = x, x$). In this way, we may select desired coherences by cycling of a phase of a spin (S) to which one set of spins (I) is sensitive and the other (I') is not. It may be noted that the more common form of spin echo difference experiments does not use 180° pulse on the S spin. More extensive applications of phase cycling in the context of coherence transfer pathway selection will follow in the sections on HSQC and HMQC.

Pulsed Field Gradients

A pulsed field gradient (23, 24) is a short, timed pulse during which the B_0 field is made spatially inhomogeneous. As a result, transverse magnetization dephases across the sample and is apparently lost. This loss, however, can be reversed by the application of a subsequent gradient, thus restoring the magnetization. A spatial average over all isochromates is taken during acquisition.

Pulsed field gradients (PFGs) are routinely used in NMR imaging (24) as well as in high-resolution,

multidimensional NMR studies of molecules in solution (25–29). The basis of pulse field gradients is described below.

Gradient Methodology

Gradient methodology is used extensively for two purposes, either rephasing (selection) (30, 31) or dephasing (elimination) (32) of particular magnetization transfer pathway.

Whenever gradients are applied in a particular direction (it is assumed here that gradients are applied along the z direction), it generates a phase factor associated with the coherence level. A brief introduction is provided to four important applications (32) of gradients that directly related to phase cycling. To describe the effects of field gradients, it is convenient to re-express the Cartesian operators I_X and I_Y in terms of raising and lowering operators I^+ and I^- (7, 22, 32–34), respectively (Appendix, Scheme V).

(A) Rephasing of Transverse Magnetization. If two gradients with the same strength, shape, duration, and polarity are applied on either side of 180° pulse [Fig. 4(A)], then transverse magnetization is refocused. Longitudinal magnetization generated (example, $I_X \rightarrow I_Z$) due to an imperfect 180° pulse will be dephased. Two cases are discussed.

Case (1): Rephasing of transverse magnetization.

$$\begin{aligned} (a \rightarrow b) \quad I^+ + I^- &\xrightarrow{\gamma_I G r \tau I_Z} I^+ \exp(-i\gamma_I G r \tau) + I^- \exp(+i\gamma_I G r \tau) \\ (b \rightarrow c) &\xrightarrow{(180^\circ) I_X} I^- \exp(-i\gamma_I G r \tau) + I^+ \exp(+i\gamma_I G r \tau) \\ (c \rightarrow d) &\xrightarrow{\gamma_I G r \tau I_Z} I^- \exp(+i\gamma_I G r \tau) \exp(-i\gamma_I G r \tau) \\ &\quad + I^+ \exp(+i\gamma_I G r \tau) \exp(-i\gamma_I G r \tau) = I^+ + I^- \quad [3a] \end{aligned}$$

The net phase acquired after 2τ is zero, and we obtain the same transverse magnetization ($I^+ + I^-$) that we started with, where G is the gradient strength, τ is the duration of gradient application, r the distance from the gradient isocenter, and γ_I and γ_S are the nuclear gyromagnetic ratio of I - and S -spin, respectively.

Case (2): Removal of artifacts (e.g., $I_X \rightarrow I_Z$) due to imperfect 180° pulse.

$$\begin{aligned} (a \rightarrow b) \quad I^+ + I^- &\xrightarrow{\gamma_I G r \tau I_Z} I^+ \exp(-i\gamma_I G r \tau) + I^- \exp(+i\gamma_I G r \tau) \end{aligned}$$

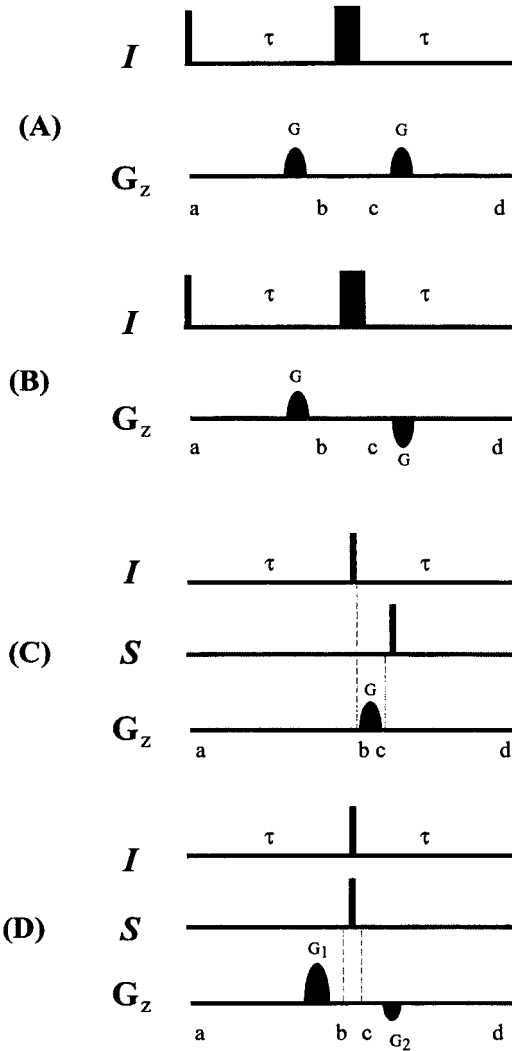


Figure 4 Application of pulsed field gradient. (A) Rephasing of transverse magnetization refocused by 180° pulse. (B) Elimination of transverse I_x or I_y components due to imperfect 180° decoupling pulse on I -spin. (C) Suppression of I - and S -spin coherences. (D) Selection of $I^+ \rightarrow S^+$ coherence order (32).

$$\begin{aligned}
 (b \rightarrow c) & \xrightarrow[\text{(imperfect pulse)}]{(180^\circ + \theta)I_x} \\
 & \cos \theta [I^+ \exp(+i\gamma_I Gr\tau) + I^- \exp(-i\gamma_I Gr\tau)] \\
 & \quad + iI_Z [\exp(-i\gamma_I Gr\tau) - \exp(+i\gamma_I Gr\tau)] \\
 (c \rightarrow d) & \xrightarrow{\gamma_I Gr\tau I_Z} \cos \theta [I^+ + I^-] \\
 & \quad + iI_Z [\exp(-i\gamma_I Gr\tau) - \exp(+i\gamma_I Gr\tau)]
 \end{aligned}$$

Any magnetization associated with a phase factor experiences different gradient strength and the overall integrals become zero. Hence, at the end of 2τ longi-

tudinal magnetization (I_Z) associated with the phase factor will be dephased.

(B) Removal of Transverse Magnetization. If two gradients with the same strength, shape and duration, but opposite polarity, are applied on either side of the 180° pulse [Fig. 4(B)], then any unwanted transverse magnetization (ex. $I_x \rightarrow I_x$ or $I_z \rightarrow I_x$) is dephased [Eq. 3b].

(Case 1): Removal of any transverse ($I_x \rightarrow I_x$) magnetization.

$$\begin{aligned}
 (a \rightarrow b) & \xrightarrow{\gamma_I Gr\tau I_Z} I^+ + I^- \\
 & \quad I^+ \exp(-i\gamma_I Gr\tau) + I^- \exp(+i\gamma_I Gr\tau) \\
 (b \rightarrow c) & \xrightarrow{(180^\circ)I_x} \\
 & \quad I^- \exp(-i\gamma_I Gr\tau) + I^+ \exp(+i\gamma_I Gr\tau) \\
 (c \rightarrow d) & \xrightarrow{\gamma_I (-G)r\tau I_Z} I^- \exp(-i\gamma_I Gr\tau) \exp(-i\gamma_I Gr\tau) \\
 & \quad + I^+ \exp(+i\gamma_I Gr\tau) \exp(+i\gamma_I Gr\tau) \\
 & = I^- \exp(-2i\gamma_I Gr\tau) + I^+ \exp(+2i\gamma_I Gr\tau) \quad [3b]
 \end{aligned}$$

The negative sign in front of the gradient means opposite polarity compared with the first gradient. At the end of the 2τ , transverse magnetization acquires a phase factor of $\exp(-2i\gamma_I Gr\tau)$ and $\exp(+2i\gamma_I Gr\tau)$ and eventually gets dephased.

(Case 2): Removal of transverse ($I_z \rightarrow I_x$) magnetization from pulse imperfections.

$$\begin{aligned}
 (a \rightarrow b) & \xrightarrow{\gamma_I Gr\tau I_Z} I_Z \\
 (b \rightarrow c) & \xrightarrow[\text{(imperfect pulse)}]{(180^\circ + \theta)I_x} I_Z \cos \theta - i/2 \sin \theta [I^+ + I^-] \\
 (c \rightarrow d) & \xrightarrow{\gamma_I (-G)r\tau I_Z} I_Z \cos \theta \\
 & \quad - i/2 \sin \theta [I^+ \exp(+i\gamma_I Gr\tau) + I^- \exp(-i\gamma_I Gr\tau)] \quad [3c]
 \end{aligned}$$

Unwanted transverse magnetization created by the imperfect 180° pulse acquires a phase factor from the second gradient and is dephased.

(C) Suppression of I- and S-Spin Coherences and Retention of Two-Spin Order ($2I_Z S_Z$). A pair of 90° pulses [Fig. 4(C)] are applied simultaneously to accomplish magnetization transfer frequently between two J -coupled I and S . However, a delay that is much

shorter than T_1 relaxation time of the coupled nuclei may be inserted between the two 90° pulses without affecting the sensitivity of the experiment. This spoiler gradient removes any accidentally excited magnetization and retains the two-spin order ($2I_ZS_Z$). This is explained as follows:

$$\begin{aligned}
 (a \rightarrow b) \quad & 2S_ZI_X \xrightarrow{(90^\circ)I_Y} -2S_ZI_Z \\
 (b \rightarrow c) \quad & \xrightarrow{\gamma_I G r \tau I_Z} -2S_ZI_Z \\
 (c \rightarrow d) \quad & \xrightarrow{(90^\circ)S_X} 2S_YI_Z \quad [3d]
 \end{aligned}$$

However, any unwanted transverse I_Y magnetization

$$\begin{aligned}
 I_Y & \xrightarrow{(90^\circ)I_Y} I_Y \xrightarrow{\gamma_I G r \tau I_Z} \\
 & -i/2[I^+ \exp(-\gamma_I G r \tau) - I^- \exp(+\gamma_I G r \tau)] \xrightarrow{(90^\circ)S_Y} \\
 & -i/2[I^+ \exp(-\gamma_I G r \tau) - I^- \exp(+\gamma_I G r \tau)] \quad [3e]
 \end{aligned}$$

acquires a phase factor and ultimately gets dephased.

(D) Selection of $I^+ \rightarrow S^+$ Coherence Order. In this gradient setup [Fig. 4(D)] $I^+ \rightarrow S^+$ coherence order is selected. The magnetization I^+ acquires a phase factor $\exp(\gamma_I G_1 r \tau)$ from the first gradient of strength (G_1). S^+ coherence is created by 90° (X) pulse on S -spin, acquires a phase of $\exp(-\gamma_S G_2 r \tau)$ from the second gradient of strength (G_2).

$$\begin{aligned}
 (a \rightarrow b) \quad & S_ZI^+ \xrightarrow{\gamma_I G_1 r \tau I_Z} S_ZI^+ \exp(-i\gamma_I G_1 r \tau) \\
 (b \rightarrow c) \quad & \xrightarrow{(90^\circ)I_X + S_X} 1/2I_Z(S^- - S^+) \exp(-i\gamma_I G_1 r \tau) \\
 & -i/4(S^- - S^+)(I^- + I^+) \exp(-i\gamma_I G_1 r \tau) \\
 (c \rightarrow d) \quad & \xrightarrow{\gamma_S G_2 r \tau S_Z} \\
 & 1/2I_ZS^- \exp(-i\gamma_I G_1 r \tau) \exp(-i\gamma_S G_2 r \tau) \\
 & -1/2I_ZS^+ \exp(-i\gamma_I G_1 r \tau) \exp(+i\gamma_S G_2 r \tau) \quad [3f]
 \end{aligned}$$

The net phase factor acquired in this coherence transfer is $\exp[-i r \tau (\gamma_I G_1 + \gamma_S G_2)]$. In order to select the coherence transfer pathway $I^+ \rightarrow S^+$ net phase acquired should be zero.

$$\begin{aligned}
 \gamma_I G_1 r \tau + \gamma_S G_2 r \tau &= 0 \\
 G_1/G_2 &= -\gamma_S/\gamma_I \quad [4]
 \end{aligned}$$

Hence for $S = {}^{15}\text{N}$ and $I = {}^1\text{H}$, for which $\gamma_I/\gamma_S = 10$, G_1 needs to be $10 \times G_2$ and of opposite polarity in order to achieve refocusing of $I^+ \rightarrow S^+$ coherence transfer.

Echo and Anti-Echo Method. One of the consequences of using pulsed-field gradients for coherence pathway selection is that 2D spectra are phase modulated, which give rise to undesirable phase-twisted line shapes. In order to obtain “phase-sensitive,” or pure, absorption more spectra, the following protocol (27, 31, 35) is adopted. Two spectra are recorded, the first being the P -type or anti-echo spectrum:

$$S(t_1, t_2)_P = \gamma \exp(i\Omega_S t_1) \exp(i\Omega_I t_2)$$

The “ P ” indicates positive, meaning here that the sign of the frequencies in ω_1 and ω_2 dimensions are the same.

The second data set is called the echo or N -type:

$$S(t_1, t_2)_N = \gamma \exp(-i\Omega_S t_1) \exp(i\Omega_I t_2)$$

The “ N ” indicates negative, meaning here that the sign of the frequencies in ω_1 and ω_2 dimensions are opposite. The P - and N -type data are stored separately; adding them together produces a cosine-modulated data set: $\cos(\Omega_S t_1) \exp(i\Omega_I t_2)$, whereas, subtracting them from one another produces a sine-modulated data set: $\sin(\Omega_S t_1) \exp(i\Omega_I t_2)$. The linear combination can be represented as follows:

$$\begin{aligned}
 & \cos(\Omega_S t_1) \exp(i\Omega_I t_2) \\
 &= 1/2\{\exp(i\Omega_S t_1) + \exp(-i\Omega_S t_1)\} \exp(i\Omega_I t_2); \\
 & \sin(\Omega_S t_1) \exp(i\Omega_I t_2) \\
 &= -i/2\{\exp(i\Omega_S t_1) - \exp(-i\Omega_S t_1)\} \exp(i\Omega_I t_2).
 \end{aligned}$$

This net data can then be processed in the usual manner by the STATES method (36).

In this section we have seen that both phase cycling and PFGs can be used for coherence pathway selection. In general, PFG-based experiments have several advantages over their phase-cycled counterparts. Before discussing these benefits, we first describe the basic, phase-cycled versions of the HSQC and HMQC experiments followed by their corresponding gradient-“enhanced” versions. Subsequently, we shall discuss sensitivity-enhanced modifications of these experiments.

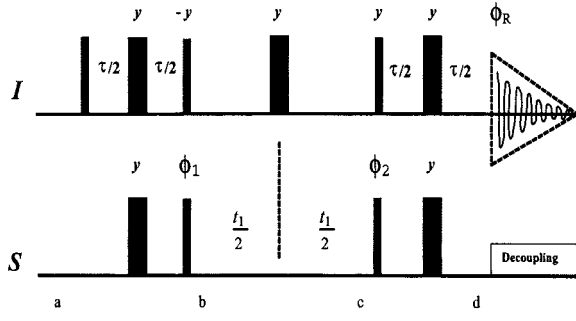


Figure 5 Pulse sequences for the fundamental HSQC sequence. The delay τ is set to $1/(2J_{IS})$. Decoupling of the S -spins during acquisition is accomplished using Waltz-16 (57). The basic phase cycling is $\phi_1(x, -x, x, -x)$, $\phi_2(x, x, -x, -x)$, and receiver $\phi_R(x, -x, -x, x)$ is applied in the sequence (39).

HETERONUCLEAR SINGLE QUANTUM CORRELATION

Although the HSQC experiment was developed after HMQC, the HSQC experiment is simpler to describe. The pulse sequence for a basic HSQC experiment (12) is shown in Fig. 5. The experiment employs two INEPT (37) magnetization transfers. The first one creates antiphase heteronuclear coherence ($I_Y \rightarrow 2I_ZS_Y$) and the second is used to convert this coherence back to observable magnetization ($2I_ZS_Y \rightarrow I_Y$). The enhancement in sensitivity possible with this scheme is significantly higher than the enhancement obtained using the nuclear Overhauser effect to observe the low- γ_S -spin resonance. It can be summarized as follows:

- The first INEPT step creates a proton antiphase magnetization ($2I_XS_Z$) during τ . To refocus chemical shift modulation during this period, a 180° pulse on both spins is introduced in the middle of τ period.
- Coherence is subsequently transferred to the directly attached heteronucleus (^{15}N or ^{13}C , etc.) by simultaneous 90° pulses on both spins ($2I_ZS_Y$).

- The S -spin coherence is frequency-labeled during the t_1 period. The 180° pulse on the I -spin in the middle of t_1 refocuses the evolution of heteronuclear J_{IS} coupling.
- A 90° pulse on both spins transfer the magnetization back to proton as antiphase I -spin magnetization ($2I_YS_Z$).
- The final spin-echo period converts this antiphase term into in-phase proton magnetization ($2I_YS_Z \rightarrow I_X$).

For a two-spin I - S system the entire sequence of events, in terms of product operators, is presented below starting from points a to d in Eq. [5].

$$\begin{aligned}
 (a \rightarrow b) \quad & I_Z \xrightarrow{(90^\circ)I_X} -I_Y \xrightarrow{2J_{IS}I_ZS_Z} \\
 & -I_Y \cos \pi J_{IS}\tau + 2I_XS_Z \sin \pi J_{IS}\tau \\
 & \xrightarrow{\tau = 1/2J_{IS}} 2I_XS_Z \xrightarrow{(90^\circ)(I_Y + S_Y)} -2I_ZS_Y \\
 (b \rightarrow c) \quad & \xrightarrow[(180^\circ)I_Y]{(\Omega_S t_1)S_Z} 2I_ZS_Y \cos \Omega_S t_1 - 2I_ZS_X \sin \Omega_S t_1 \\
 (c \rightarrow d) \quad & \xrightarrow{(90^\circ)(I_Y + S_X)} 2I_XS_Z \cos \Omega_S t_1 - 2I_XS_X \sin \Omega_S t_1 \\
 & \xrightarrow[\tau = 1/2J_{IS}]{2J_{IS}I_ZS_Z} I_Y \cos \Omega_S t_1 - 2I_XS_X \sin \Omega_S t_1 \quad [5]
 \end{aligned}$$

Therefore, prior to detection (point d) there is in-phase magnetization I_Y as well as an unobservable multiple quantum term $2I_XS_X$. A basic two-step phase cycle is necessary to filter out the undesirable magnetization from protons attached to ^{12}C or ^{14}N and a four-step cycle for complete elimination of undesirable double quantum terms. A two-step phase cycle can not eliminate unwanted double quantum terms. Details of the four-step phase cycling scheme (38) are provided in Table 1.

Table 1 Phase Cycling Used in Basic HSQC Pulse Sequence

	ϕ_1	ϕ_2	ϕ_R	Magnetization at Point d Protons Bound to ^{13}C	Magnetization at Point d for Protons Bound to ^{12}C
Step I	x	x	x	$I_Y \cos \pi J_{IS}t_1 - 2I_XS_X \sin \pi J_{IS}t_1$	I_Y
Step II	$-x$	x	$-x$	$-(I_Y \cos \pi J_{IS}t_1 - 2I_XS_X \sin \pi J_{IS}t_1)$	I_Y
Step III	x	$-x$	$-x$	$-(I_Y \cos \pi J_{IS}t_1 + 2I_XS_X \sin \pi J_{IS}t_1)$	I_Y
Step IV	$-x$	$-x$	x	$I_Y \cos \pi J_{IS}t_1 + 2I_XS_X \sin \pi J_{IS}t_1$	I_Y

Magnetization before the start of acquisition is shown for protons attached to ^{12}C and ^{13}C (Fig. 5).

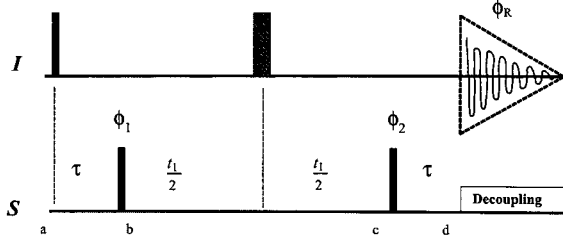


Figure 6 Pulse sequence for the fundamental HMQC sequence. τ is set to $1/(2J_{IS})$. Phase of the 90° pulse on S -spin and the receiver are $\phi_1(x, -x, x, -x)$, $\phi_2(x, x, -x, -x)$, and $\phi_R(x, -x, -x, x)$, respectively. Points (a–d) are meant to describe magnetization in the pulse sequence. The dashed bar refers to 180° pulse on I -spin (39).

HETERONUCLEAR MULTIPLE QUANTUM CORRELATION

The HMQC experiment provides correlation between protons and scalar coupled heteronuclei (10) through the creation of heteronuclear multiple-quantum coherence. The pulse sequence for the basic HMQC scheme (10, 11) is shown in Fig. 6. Its components are as follows:

- The HMQC pulse sequence starts with a 90° pulse on the I -spin followed by a delay $\tau = 1/2J_{IS}$. As a result, in-phase I magnetization is converted into antiphase ($2I_Y S_Z$) magnetization. Because the centrally placed 180° pulse on the I -spin refocuses the proton chemical shift evolution over the entire duration of the sequence, we need to consider only J -evolution as far as spin I is concerned.
- A 90° pulse on the S -spin converts this antiphase term into a combination of zero- and double-quantum coherence ($2I_Y S_X$).
- This coherence evolves during the t_1 evolution period. In the absence of the 180° I -spin pulse in the center of the t_1 period, the $I_Y S_X$ term would have evolved with the sum ($\Omega_I + \Omega_S$) and difference ($\Omega_I - \Omega_S$) frequencies of the two spins. However, the centrally placed 180° pulse on the I -spin selectively refocuses I -spin chemical shift evolution and, therefore, the coherence is labeled only with the S -spin frequency.
- The second 90° pulse on the S -spin “returns” the multiple quantum coherence to observable antiphase I -spin magnetization.
- Finally the second delay τ converts the antiphase term into an in-phase term.

Steps (a–d) are described below using a product operator analysis:

$$\begin{aligned}
 (a \rightarrow b) \quad I_Z &\xrightarrow{(90^\circ)I_X} -I_Y \xrightarrow[\tau = 1/(2J_{IS})]{2J_{IS}I_Z S_Z} 2I_X S_Z + 2I_Y S_Z \xrightarrow{(90^\circ)S_X} -2I_X S_Y \\
 (b \rightarrow c) \quad &\xrightarrow[(\Omega_S t_1)S_Z]{(\Omega_I t_1)I_Z} -2I_X S_Y \cos \Omega_I t_1 \cos \Omega_S t_1 \\
 &\quad + 2I_X S_X \cos \Omega_I t_1 \sin \Omega_S t_1 - 2I_Y S_Y \sin \Omega_I t_1 \cos \Omega_S t_1 \\
 &\quad + 2I_Y S_X \sin \Omega_I t_1 \sin \Omega_S t_1 \\
 (c \rightarrow d) \quad &\xrightarrow{(90^\circ)S_X} 2I_X S_X \cos \Omega_I t_1 \sin \Omega_S t_1 \\
 &\quad + 2I_Y S_X \sin \Omega_I t_1 \sin \Omega_S t_1 - 2I_X S_Z \cos \Omega_I t_1 \cos \Omega_S t_1 \\
 &\quad - 2I_Y S_Z \sin \Omega_I t_1 \cos \Omega_S t_1 \\
 &\xrightarrow[(\tau = 1/2J_{IS})]{2J_{IS}I_Z S_Z} 2I_X S_X \cos \Omega_I t_1 \sin \Omega_S t_1 \\
 &\quad + 2I_Y S_X \sin \Omega_I t_1 \sin \Omega_S t_1 - I_Y \cos \Omega_I t_1 \cos \Omega_S t_1 \\
 &\quad + I_X \sin \Omega_I t_1 \cos \Omega_S t_1 \quad [6a]
 \end{aligned}$$

The 180° pulse of I -spin in the middle of t_1 refocuses the I -spin chemical shift. As a result, magnetization transfer from points a to d is as follows:

$$\begin{aligned}
 (b \rightarrow c) \quad &\xrightarrow[(\Omega_S t_1)S_Z]{(180^\circ)I_X} -2I_X (S_Y \cos \Omega_S t_1 - S_X \sin \Omega_S t_1) \\
 (c \rightarrow d) \quad &\xrightarrow{(90^\circ)S_X} -2I_X S_Z \cos \Omega_S t_1 + 2I_X S_X \sin \Omega_S t_1 \\
 &\xrightarrow[(\tau = 1/2J_{IS})]{2J_{IS}I_Z S_Z} -I_Y \cos \Omega_S t_1 + 2I_X S_X \sin \Omega_S t_1 \quad [6b]
 \end{aligned}$$

Experimentally one can detect only single quantum coherence (I_X , I_Y , $I_X S_Z$, $I_Y S_Z$), whereas multiple quantum ($I_X S_Y$, $I_X S_X$, $I_Y S_Y$, $I_Y S_X$) remains undetectable. This unobservable coherence can be converted into observable single-quantum magnetization with a modified pulse sequence called sensitivity-enhanced HMQC (se-HMQC). In the HMQC sequence, unwanted magnetization transfer pathways are removed by a four-step phase cycle (Table 2).

Sensitivity Enhancement in Heteronuclear Experiments

The sensitivity of proton-detected 2D heteronuclear correlation NMR spectroscopy can be increased as much as a factor of $\sqrt{2}$ compared with the phase-cycled method for heteronuclei with a single attached proton. This enhanced sensitivity is obtained by refo-

Table 2 Phase Cycling Used in Basic HMQC Pulse Sequence

	ϕ_1	ϕ_2	ϕ_R	Magnetization at Point d Protons Bound to ^{13}C	Magnetization at Point d for Protons Bound to ^{12}C
Step I	x	x	x	$-I_Y \cos \pi J_{IS} t_1 + 2I_X S_X \sin \pi J_{IS} t_1$	$-I_Y$
Step II	$-x$	x	$-x$	$-(-I_Y \cos \pi J_{IS} t_1 + 2I_X S_X \sin \pi J_{IS} t_1)$	$-I_Y$
Step III	x	$-x$	$-x$	$I_Y \cos \pi J_{IS} t_1 + 2I_X S_X \sin \pi J_{IS} t_1$	$-I_Y$
Step IV	$-x$	$-x$	x	$-(I_Y \cos \pi J_{IS} t_1 + 2I_X S_X \sin \pi J_{IS} t_1)$	$-I_Y$

Magnetization before the start of acquisition is shown for protons attached to ^{12}C and ^{13}C (Fig. 6).

cusing and detecting two orthogonal in-phase magnetization components (36, 38, 39).

Sensitivity-enhanced HSQC (se-HSQC) Sequence.

In the conventional HSQC sequence, heteronuclear single quantum evolves under the influence of the S -spin chemical shift during t_1 to yield two-orthogonal terms proportional to $2I_Z S_Y$ and $2I_Z S_X$. One of the two antiphase magnetization terms is not refocused by the reverse INEPT sequence and consequently does not contribute to the final observed magnetization. Therefore, on average one-half of the initial I -spin polarization does not contribute to the detected signal. In contrast, the sensitivity-enhanced versions of these experiments enhance the S/N ratio by $\sqrt{2}$ relative to the phase-cycled version.

The pulse sequence for the sensitivity-enhanced HSQC (36, 38, 39) is shown in Fig. 7. Magnetization at different points (a–f) for I - S spin system are described below:

$$\begin{aligned}
 (a \rightarrow b) \quad & I_Z \xrightarrow{(90^\circ)I_X} -I_Y \xrightarrow{2J_{IS}I_ZS_Z} \\
 & -I_Y \cos \pi J_{IS} \tau + 2I_X S_Z \sin \pi J_{IS} \tau \\
 & \xrightarrow{\tau = 1/2J_{IS}} 2I_X S_Z \xrightarrow{(90^\circ)(I_- + S_X)} -2I_Z S_Y \\
 (b \rightarrow c) \quad & \xrightarrow[(\Omega_S)S_Z]{(180^\circ)I_Y} 2I_Z S_Y \cos \Omega_S t_1 - 2I_Z S_X \sin \Omega_S t_1 \\
 (c \rightarrow d) \quad & \xrightarrow[(90^\circ)I_Y S_X]{(90^\circ)I_Y S_X} 2I_X S_Z \cos \Omega_S t_1 - 2I_X S_X \sin \Omega_S t_1 \\
 & \xrightarrow[\tau = 1/2J_{IS}]{2J_{IS}I_ZS_Z} I_Y \cos \Omega_S t_1 - 2I_X S_X \sin \Omega_S t_1 \\
 (d \rightarrow e) \quad & \xrightarrow[(90^\circ)I_Y S_Y]{(90^\circ)I_Y S_Y} I_Z \cos \Omega_S t_1 + 2I_X S_Z \sin \Omega_S t_1 \\
 & \xrightarrow[\tau = 1/2J_{IS}]{2J_{IS}I_ZS_Z} -I_Z \cos \Omega_S t_1 + I_Y \sin \Omega_S t_1 \\
 (e \rightarrow f) \quad & \xrightarrow{(90^\circ)I_Y} -I_X \cos \Omega_S t_1 + I_Y \sin \Omega_S t_1 \quad [7]
 \end{aligned}$$

The results from this analysis can be generalized as follows. The observable magnetization prior to detection for the first experiment is

$$-I_X \cos \Omega_S t_1 + \delta_{1n} I_Y \sin \Omega_S t_1 \quad [8]$$

and for the second experiment is

$$I_X \cos \Omega_S t_1 + \delta_{1n} I_Y \sin \Omega_S t_1 \quad [9]$$

where δ_{1n} is the Kronecker delta and n is the number of protons directly attached to the heteronucleus. This idea was originally proposed by Rance et al. (36, 38, 40) as the preservation of equivalent pathways (PEP) technique. For $n = 1$, the observable magnetization ($-I_X \cos \Omega_S t_1 + I_Y \sin \Omega_S t_1$) represents orthogonal in-phase I -spin magnetization components, that have both evolved at the frequency of S -spin during t_1 . Therefore, the entire initial I -spin polarization contributes to the observed signal, resulting in a sensitivity enhancement compared with the conventional HSQC sequence. In the postacquisition data processing (Table 3) scheme data from step (I) and step (II) are kept separate. On

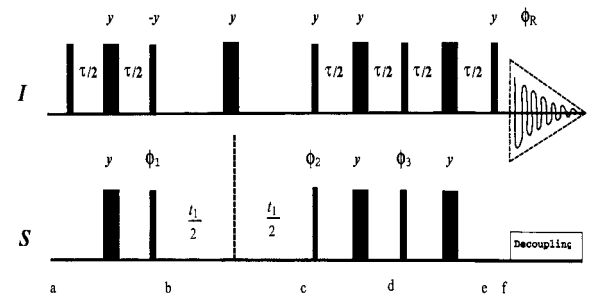


Figure 7 Pulse sequence for the heteronuclear single quantum spectra with enhanced sensitivity (se-HSQC). Magnetization at different points (a–f) is described in the text. Decoupling in heteronuclear channel is done by Waltz-16 (57). The delay τ is set to $1/2J_{IS}$. Quadrature detection in ω_1 dimension is achieved by TPPI (49) or by STATES method (36). The basic phase cycling is $\phi_1(x, -x, x, -x)$, $\phi_2(x, x, -x, -x)$, $\phi_3(y, -y, y, -y)$, and receiver phase $\phi_R(x, -x, -x, x)$. Net magnetization before acquisition is given in Table 3.

Table 3 Four-Step Phase Cycles Are Used in Sensitivity-Enhanced HSQC Sequence

	ϕ_1	ϕ_2	ϕ_3	ϕ_R	Magnetization at Point (f)
Step I	x	x	y	x	$-I_X \cos \Omega_S t_1 + I_Y \sin \Omega_S t_1$
Step II	$-x$	x	$-y$	$-x$	$-(-I_X \cos \Omega_S t_1 - I_Y \sin \Omega_S t_1)$
Step III	x	$-x$	y	$-x$	$I_X \cos \Omega_S t_1 + I_Y \sin \Omega_S t_1$
Step IV	$-x$	$-x$	$-y$	x	$-(I_X \cos \Omega_S t_1 - I_Y \sin \Omega_S t_1)$

Magnetization prior to acquisition point (f) is shown in every step (Fig. 7).

subtraction, the two data sets give the single observable term (SUBTRACT spectra):

$$2I_X \cos \Omega_S t_1 \quad [10]$$

On addition (step II + step I), the two data sets yield the single observable term (ADD spectra):

$$2I_Y \sin \Omega_S t_1 \quad [11]$$

The coefficient of 2 in the above equations arises because two acquisitions have been performed. In practice, each experiment would be recorded with one-half of the total number of transients desired to maintain the same total acquisition time as the conventional, phase-cycled experiment. The data sets described in Eqs. [10] and [11] are identical except for a 90° phase difference in both dimensions. The data sets can be transformed and phased into 2D heteronuclear correlation spectra with purely absorptive peak shapes in both dimensions (38).

In adding and subtracting these data sets, the noise also increases by a factor $\sqrt{2}$ and, therefore, the S/N increases by a factor $2/\sqrt{2} = \sqrt{2} \sim 1.4$. In practice, the theoretical S/N enhancement of 40% is never achieved, because the pulse sequence consists of additional pulses and delays that tend to degrade the sensitivity below the theoretical maximum. Even so, in most cases the S/N enhancement is sufficient to warrant routine incorporation of this sequence into more complex pulse sequences.

Figure 8 shows 1D slices parallel to the ω_2 axis for selected N-H resonances from 2D spectra. Cross sections are shown for the amide resonances of (a) Tyr²³, (b) Ala²⁵, (c) Leu²⁹, and (d) side-chain NH₂ with a ¹⁵N chemical shift of 115 PPM. In each case the bottom trace is taken from the conventional HSQC spectrum, the second trace from the ADD spectrum, the third trace from the SUBTRACT spectrum, and the top trace from the enhanced spectrum. Slices are plotted on the same absolute intensity scale. In each case the sensitivity improvement of the enhanced spectrum over the original spectrum is 1.26 for Fig. 8(a), 1.26 for Fig. 8(b), and 1.31 for Fig. 8(c).

Sensitivity-enhanced HMQC Sequence. The se-HMQC sequence (38, 39) works in virtually the same way as the se-HSQC sequence. Enhanced sensitivity is obtained by refocusing and detecting two-orthogonal in-phase proton magnetization components, rather than a single component. The two magnetization components are deconvoluted to produce two pure-phase spectra with an enhanced sensitivity compared with the fundamental HMQC sequence. The pulse sequence for the se-HMQC (Fig. 9) and detailed analysis of magnetization at different points (a-i) is given below:

$$(a \rightarrow b) \quad I_Z \xrightarrow{(90^\circ)I_X} -I_Y \xrightarrow{(\Omega_I \tau)I_Z} -I_Y \cos \Omega_I \tau + I_X \sin \Omega_I \tau$$

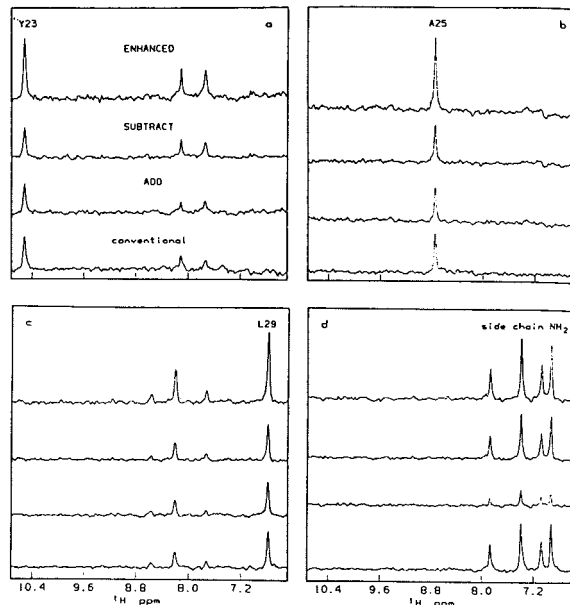


Figure 8 Cross section from ¹H-¹⁵N spectra of BPTI. Cross sections are shown for the amide resonance of (a) Tyr²³, (b) Ala²⁵, (c) Leu²⁹ and (d) side-chain NH₂ resonance. In each case the bottom trace is taken from the conventional HSQC spectrum, the second trace from the add spectrum, the third trace from the subtract spectrum, and the top trace from the enhanced spectrum. The slices are plotted on an absolute intensity scale (38).

$$\xrightarrow{2J_{IS}I_ZS_Z} \cos \Omega_I \tau [-I_Y \cos \pi J_{IS} \tau + 2I_X S_Z \sin \pi J_{IS} \tau] \\ + \sin \Omega_I \tau [I_X \cos \pi J_{IS} \tau + 2I_Y S_Z \sin \pi J_{IS} \tau]$$

In order to create maximum anti-phase magnetization, τ is set to $(1/2J_{IS})$:

$$\xrightarrow{\tau = 1/2J_{IS}} 2I_X S_Z \cos \Omega_I \tau - 2I_Y S_Z \sin \Omega_I \tau \\ \xrightarrow{(90^\circ)S_X} -2I_X S_Y \cos \Omega_I \tau - 2I_Y S_Y \sin \Omega_I \tau \\ (b \rightarrow c) \xrightarrow[(\Omega_S t_1)S_Z]{(180^\circ)I_Y} 2I_X \cos \Omega_I \tau (S_Y \cos \Omega_S t_1 \\ - S_X \sin \Omega_S t_1) - 2I_Y \sin \Omega_I \tau (S_Y \cos \Omega_S t_1 - S_X \sin \Omega_S t_1)$$

Magnetization at this point is similar to the conventional HMQC experiment.

$$(c \rightarrow d) \xrightarrow{(90^\circ)S_X} 2I_X S_Z \cos \Omega_I \tau \cos \Omega_S t_1 \\ - 2I_Y S_Z \sin \Omega_I \tau \cos \Omega_S t_1 - 2I_X S_X \cos \Omega_I \tau \sin \Omega_S t_1 \\ + 2I_Y S_X \sin \Omega_I \tau \sin \Omega_S t_1 \xrightarrow[(\tau = 1/2J_{IS})]{(\Omega_I \tau)I_Z, 2I_Z S_Z} \\ I_Y \cos \Omega_S t_1 - 2I_X \sin \Omega_S t_1 [-S_Y \sin \Omega_S \tau + S_X \cos \Omega_S \tau] \\ (d \rightarrow e) \xrightarrow[(180^\circ)S_Y]{(90^\circ)I_X} \\ I_Z \cos \Omega_S t_1 - 2I_X \sin \Omega_S t_1 [S_Y \sin \Omega_S \tau - S_X \cos \Omega_S \tau] \\ (e \rightarrow f) \xrightarrow{(\Omega_I \tau)I_Z} I_Z \cos \Omega_S t_1 \\ + 2I_X S_X \cos \Omega_I \tau \sin \Omega_S t_1 + 2I_Y S_X \sin \Omega_I \tau \sin \Omega_S t_1 \\ (f \rightarrow g) \xrightarrow[(90^\circ)S_Y]{(180^\circ)I_Y} -I_Z \cos \Omega_S t_1 \\ + 2I_X S_Z \cos \Omega_I \tau \sin \Omega_S t_1 - 2I_Y S_Z \sin \Omega_I \tau \sin \Omega_S t_1 \\ (g \rightarrow h) \xrightarrow[(\tau = 1/2J_{IS})]{2J_{IS}I_Z S_Z} -I_Z \cos \Omega_S t_1 + I_Y \sin \Omega_S t_1 \\ (h \rightarrow i) \xrightarrow{(90^\circ)I_Y} -I_X \cos \Omega_S t_1 + I_Y \sin \Omega_S t_1 \quad [12]$$

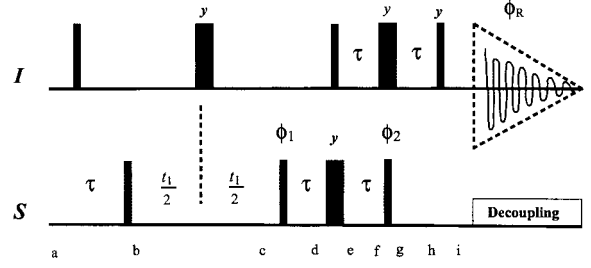


Figure 9 Pulse sequence for the heteronuclear multiple quantum spectra with enhanced-sensitivity (se-HMQC). Magnetization at different points (a–i) is described in the text. Decoupling in heteronuclear channel is done by Waltz-16 (58). The delay τ is set to $1/2J_{IS}$. Quadrature detection in ω_1 dimension is achieved by the TPPI (49) or by the STATES method (36). The basic phase cycling is $\phi_1(x, -x, -x, x)$, $\phi_2(y, -y, -y, y)$, and receiver phase $\phi_R(x, -x, -x, x)$ (39). Net magnetization before acquisition is given in Table 4.

Thus, both the orthogonal in-phase magnetization (I_X , I_Y) components are detected, thereby enhancing the sensitivity relative to a phase-cycled HMQC experiment. The net magnetization arising from each of the four steps is given in Table 4. Data processing is the same as mentioned in the se-HSQC sequence.

Gradient-Enhanced Pulse Sequences

Although phase cycling is a convenient means of coherence pathway selection, there are several pitfalls that one may encounter.

- A minimum number of scans or transients one required to achieve the desired phase cycling, thereby setting a lower limit to the total data collection time.
- Because phase cycling is essentially a subtraction procedure, artifacts may arise because of imperfect cancellation of undesirable pathways due to pulse or phase instabilities between transients. This is especially so when the concentration of I - S spin pairs is low relative to unpaired I -spin. For example, in an H-C correlation experiment at natural abundance one needs to can-

Table 4 Four-Step Phase Cycles Used in Sensitivity-Enhanced HMQC Sequence

	ϕ_1	ϕ_2	ϕ_3	ϕ_R	Magnetization at Point (i)
Step I	x	x	y	x	$-I_X \cos \Omega_S t_1 + I_Y \sin \Omega_S t_1$
Step II	$-x$	x	$-y$	$-x$	$-(-I_X \cos \Omega_S t_1 - I_Y \sin \Omega_S t_1)$
Step III	x	$-x$	y	x	$I_X \cos \Omega_S t_1 + I_Y \sin \Omega_S t_1$
Step IV	$-x$	$-x$	$-y$	$-x$	$-(I_X \cos \Omega_S t_1 - I_Y \sin \Omega_S t_1)$

Magnetization at the point (i) (Fig. 9) is shown in column 5.

cel out 99% signals from ^{12}C -bound protons by phase cycling while retaining only the remaining 1% of ^{13}C -bound protons.

- Subtraction artifacts are especially severe when dynamic range is an issue, e.g., when carrying out experiments in H_2O . In aqueous solution, even for near 100% isotope-labeled samples, one needs to phase cycle out water protons whose concentration is typically 110 molar, which is typically $\sim 10^5$ times higher than the sample concentration. However, at these concentration ratios, in order to prevent the solvent signal from “overflowing” the ADC, the receiver gain has to be lowered to a level where the signal from the sample falls below the ADC digitizer resolution, and therefore, never rises above noise level. As a result, although one achieves apparent solvent suppression from phase cycling, the desired signal from the sample is never observed. To avoid this problem, it is usually necessary to presaturate the solvent or use other solvent suppression techniques.

The use of pulsed-field gradients for coherence selection provides a powerful alternative to phase cycling (24, 41) by permitting selection of the desired coherence transfer pathway in a single transient, while simultaneously eliminating (actually, dephasing) all unwanted pathways. As a result, most of the problems associated with phase cycling are mitigated (42). The following section describes the incorporation of gradient based coherence selection in the HSQC and HMQC experiments.

Sensitivity-Enhancement with Gradients

Pulsed-field gradients are used to suppress undesirable coherence pathways and to suppress solvent in a single transient, thereby eliminating or diminishing the need for phase cycling (31, 35, 43). In a gradient-enhanced experiment, either the P - or N -type coherence is selected and this introduces a sensitivity loss by a factor of $\sqrt{2}$ compared with the fundamental experiment. However, when incorporated into a sensitivity-enhanced HSQC/HMQC scheme, as proposed by Kay et al. (44), both N -type (echo) as well as P -type (anti-echo) coherence pathways are selected and overall sensitivity is retained. The gradient versions of PEP-based, sensitivity-enhanced HSQC/HMQC sequences are often called Rance-Kay techniques.

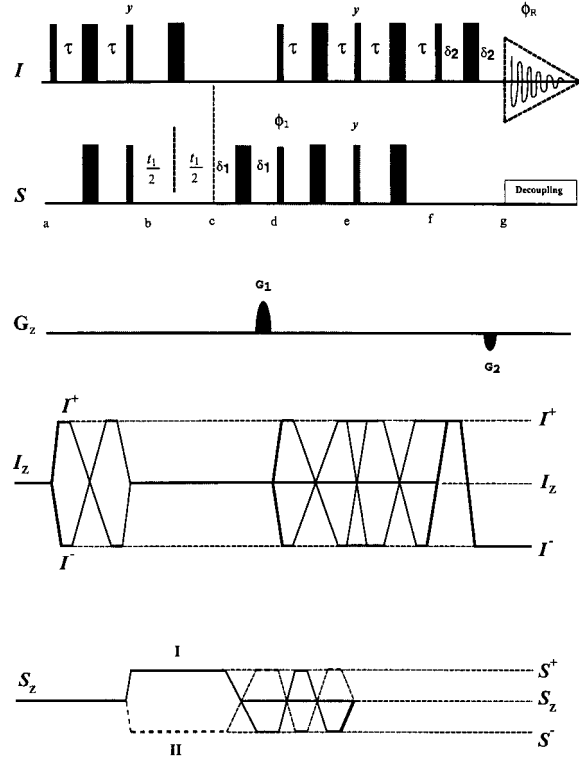


Figure 10 Pulse sequence for the gradient with sensitivity-enhanced HSQC (gs-HSQC). Phases $\phi_1(x, -x)$ and $\phi_R(x, -x)$ are used in the sequence (44). For every t_1 increment, the phase ϕ_1 and the receiver are inverted. The strength of gradients G_1 and G_2 are 30 and 29.05 G/cm with duration 2.5 and 0.25 ms, respectively, along the z direction. In these pulse sequences, the delays τ , δ_1 , δ_2 are set to 2.75, 2.75, and 0.3 ms, respectively. Decoupling is achieved with the use of the Waltz decoupling sequence (57) using a 1-kHz radio frequency field. Net magnetization at different points (a–g) are described in the text. The two coherence transfer pathways are depicted as I and II.

Gradient-Enhanced HSQC Sequence with Sensitivity Enhancement (gs-HSQC). The gradient version of the HSQC sequence with sensitivity enhancement (Fig. 10) is described below:

$$\begin{aligned}
 (a \rightarrow b) \quad & I_z \xrightarrow{(90^\circ)I_x} -I_y \xrightarrow{2J_{IS}I_zS_z} -I_y \cos \pi J_{IS}\tau \\
 & + 2I_x S_z \sin \pi J_{IS}\tau \xrightarrow{\tau = 1/2J_{IS}} 2I_x S_z \xrightarrow{(90^\circ)(I_y + S_y)} 2I_z S_y \\
 (b \rightarrow c) \quad & \xrightarrow{(\Omega_{St_1})S_z, (180^\circ)I_x} \\
 & -2I_z S_y \cos \Omega_{St_1} + 2I_z S_x \sin \Omega_{St_1} \\
 (c \rightarrow d) \quad & \xrightarrow{(90^\circ)(I_x + S_x)} 2I_y S_z \cos \Omega_{St_1} + 2I_y S_x \sin \Omega_{St_1} \\
 & \xrightarrow{(180^\circ)S_y}
 \end{aligned}$$

$$\begin{aligned}
(d \rightarrow e) & \xrightarrow[\tau = 1/2J_{IS}]{2J_{IS}I_ZS_Z} -I_X \cos \Omega_S t_1 + 2I_Y S_X \sin \Omega_S t_1 \\
(e \rightarrow f) & \xrightarrow[2J_{IS}I_ZS_Z(\tau = 1/2J_{IS})]{(90^\circ)(I_Y + S_Y)} I_Z \cos \Omega_S t_1 + I_X \sin \Omega_S t_1 \\
(f \rightarrow g) & \xrightarrow[(180^\circ)I_X]{(90^\circ)I_X} I_Y \cos \Omega_S t_1 + I_X \sin \Omega_S t_1 \quad [13]
\end{aligned}$$

For each t_1 value, two transients are recorded and stored separately. The phase ϕ_1 is incremented by 180° , and the amplitude of the second gradient pulse inverted for the second transient. Signals recorded for a given t_1 value are stored in separate locations and are added and subtracted to generate amplitude modulated signals. A 90° zero-order phase correction is subsequently applied to every second FID. In general current software processing package perform a linear combination of the two datasets in the time domain, rather than the addition and subtraction in the frequency domain. In general terms the following operation is performed. Real1 and Imag1 are the first data points of the two data sets (mostly acquired in an interleave fashion). Real2 and Imag2 are the second points or in other words the imaginary points in the acquired dimension:

$$\text{Real1} = -\text{Imag2} - \text{Imag1}$$

$$\text{Imag1} = \text{Real2} + \text{Real1}$$

$$\text{Real2} = \text{Real2} - \text{Real1}$$

$$\text{Imag2} = -\text{Imag2} - \text{Imag1}$$

The resulting data sets are transformed by the STATES method (36).

Figure 11 shows 1D cross sections at 121.3 and 119.2 PPM from ^1H - ^{15}N HSQC spectra (recorded by three different sequences) on CBD, a protein fragment of 115 amino acid residues (44). Figure 11(a,c) show spectra from the conventional HSQC sequence, and Fig. 11(b,d) shows spectra from the sensitivity-enhanced gradient sequence (gs-HSQC). The gs-HSQC sequences give sensitivity improvement of 10% compared with the fundamental HSQC sequence.

Gradient versions of se-HSQC experiments have additional advantages beyond the single-transient elimination of $I^+ \rightarrow I^-$ pathway. In a nongradient se-HSQC sequence, the two pathways are not always perfectly balanced, because they have slightly different relaxation losses, as one pathway is channeled through I_Z and the other through $2I_Y S_X$, which have different relaxation rates; these differences are more pronounced in large molecules. This means that a

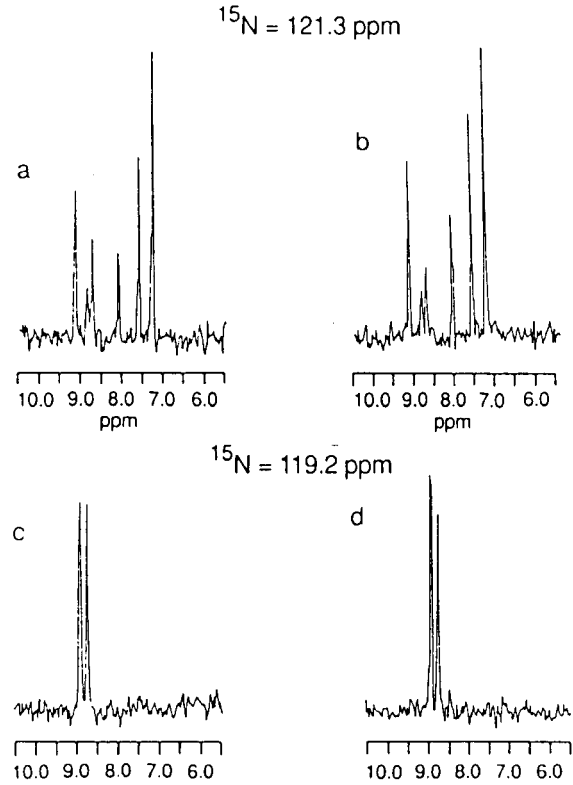


Figure 11 Cross section from ^1H - ^{15}N spectra of CBD recorded with different sequences (a,c) nongradient, nonenhanced HSQC sequence (two scan/FID, 28 Hz presentation field); (b,d) from gradient-enhanced HSQC sequence with sensitivity-enhancement (gs-HSQC; 1 transient/FID). The strength and duration of gradient pulses were identical in both the gradient experiments. Spectra are normalized so that noise level was the same for each spectrum (44).

P -type signal is contaminated with some N -type signal, and vice versa. In the PFG se-HSQC experiment these artifacts are efficiently suppressed.

Gradient-Enhanced HMQC Sequence with Sensitivity Enhancement (gs-HMQC). A gradient version for the gs-HMQC pulse sequence (45) is shown in Fig. 12 along with the coherence transfer pathway. Magnetizations at different points are shown in Eq. [14], and coherence transfer pathways are drawn based on Schemes III–IV and Scheme V, respectively, in the Appendix. The strategies in this pulse sequence design are based on those of Palmer et al. (38) and Kay et al. (44):

$$\begin{aligned}
(a \rightarrow b) \quad I_Z & \xrightarrow{(90^\circ)I_X} -I_Y \xrightarrow{2J_{IS}I_ZS_Z} \\
& -I_Y \cos 2\pi J_{IS}\tau + 2I_X S_Z \sin 2\pi J_{IS}\tau
\end{aligned}$$

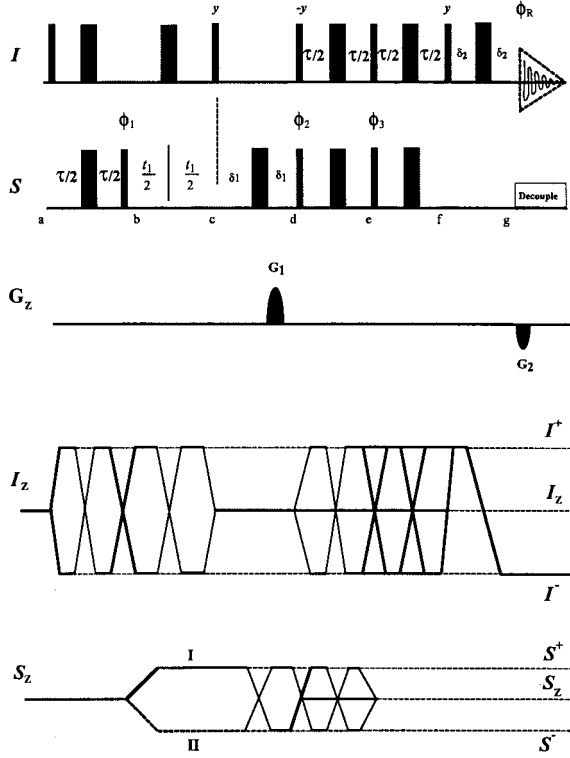


Figure 12 Pulse sequence for the gradient with sensitivity-enhanced HMQC (gs-HMQC) sequence. Phases $\phi_1(x, x, -x, -x)$, $\phi_2(x, -x)$, $\phi_3(y, -y)$, and $\phi_R(x, -x, -x, x)$ are used in the sequence (45). In these pulse sequences, the delays τ , δ_1 , and δ_2 are set to 2.77, 1.75, and 0.4 ms, respectively. Phase cycling is not necessary; however, a four-step phase cycle is used, which is $\phi_1(x, x, -x, -x)$, $\phi_2(x, -x)$, $\phi_3(y, -y)$, and receiver $\phi_R(x, -x, -x, x)$. Unlabeled pulses are applied along the x -axis. For every t_1 increment, the phase ϕ_2 and the gradient G_2 is inverted. The strength of gradients G_1 and G_2 are 40 G/cm with duration 1.5 and 0.3 ms, respectively, along the z direction. Quadrature detection in the ω_1 dimension is achieved by adding and subtracting two consecutive transients. Magnetization at different points (a–g) are also shown in the text. The two coherence transfer pathways are depicted as I and II.

$$\xrightarrow{\tau = 1/2J_{IS}} 2I_X S_Z \xrightarrow{(90^\circ)S_X} -2I_X S_Y$$

The 180° (X) pulse on I -spin refocuses the chemical shift of I -spin:

$$(b \rightarrow c) \xrightarrow{(\Omega_S t_1)S_Z} -2I_X [S_Y \cos \Omega_S t_1 - S_X \sin \Omega_S t_1]$$

$$(c \rightarrow d) \xrightarrow[(180^\circ)S_X]{(90^\circ)I_Y} 2I_Z [S_Y \cos \Omega_S t_1 + S_X \sin \Omega_S t_1]$$

$$(d \rightarrow e) \xrightarrow[(90^\circ)S_X]{(90^\circ)I_{-Y}}$$

$$2I_X S_Z \cos \Omega_S t_1 - 2I_X S_X \sin \Omega_S t_1 \xrightarrow[(\tau = 1/2J_{IS})]{2J_{IS}I_Z S_Z} + I_Y \cos \Omega_S t_1 - 2I_X S_X \sin \Omega_S t_1$$

$$(e \rightarrow f) \xrightarrow{(90^\circ)I_X S_Y} I_Z \cos \Omega_S t_1$$

$$-2I_X S_Z \sin \Omega_S t_1 \xrightarrow[(\tau = 1/2J_{IS})]{2J_{IS}I_Z S_Z} I_Z \cos \Omega_S t_1 - I_Y \sin \Omega_S t_1$$

Two orthogonal in-phase magnetization components are detected, which enhances the sensitivity of the signals.

$$(f \rightarrow g) \xrightarrow[(180^\circ)I_X]{(90^\circ)I_Y} I_X \cos \Omega_S t_1 + I_Y \sin \Omega_S t_1 \quad [14]$$

However, for each t_1 , two transients are recorded and stored separately; corresponding to $\phi_2 = x$, $\phi_2 = -x$. The net magnetization for each step before the acquisition (point g) is given below.

$$\text{Step I} \quad I_X \cos \Omega_S t_1 + I_Y \sin \Omega_S t_1 \quad \text{if } \phi_2 = x \quad [15a]$$

$$\text{Step II} \quad -I_X \cos \Omega_S t_1 + I_Y \cos \Omega_S t_1 \quad \text{if } \phi_2 = -x \quad [15b]$$

The selection of coherence transfer pathways is accomplished with two gradients, G_1 and G_2 .

Pathway I ($S^+ \rightarrow I^-$) and Pathway II ($S^- \rightarrow I^-$). The net phase acquired from the two pathways is as follows:

$$\pm \gamma_S \tau_1 G_1 - \gamma_I \tau_2 G_2 = 0. \quad [16]$$

where γ_S and γ_I are the gyromagnetic ratio of S - and I -spin, τ_1 and τ_2 are the duration of the first and second gradients, and G_1 and G_2 are the gradient strengths. The refocusing condition is

$$\pm \frac{\tau_1 G_1}{\tau_2 G_2} = \frac{\gamma_I}{\gamma_S} \quad [17]$$

for ^1H - ^{15}N , $\gamma_I/\gamma_S \approx 10$, $\tau_1 G_1 = \pm 10 \tau_2 G_2$. By adjustment of the gradient strength, duration, and polarity, echo (pathway I) as well as anti-echo (pathway II) signals are selected.

For each t_1 value, two transients corresponding to $\phi_2 = x$ (Eq. 15a) and $\phi_2 = -x$ (Eq. 15b) are recorded and stored separately and then added and subtracted, with a 90° phase shift applied to the addition of the transients. Final pure phase absorption is

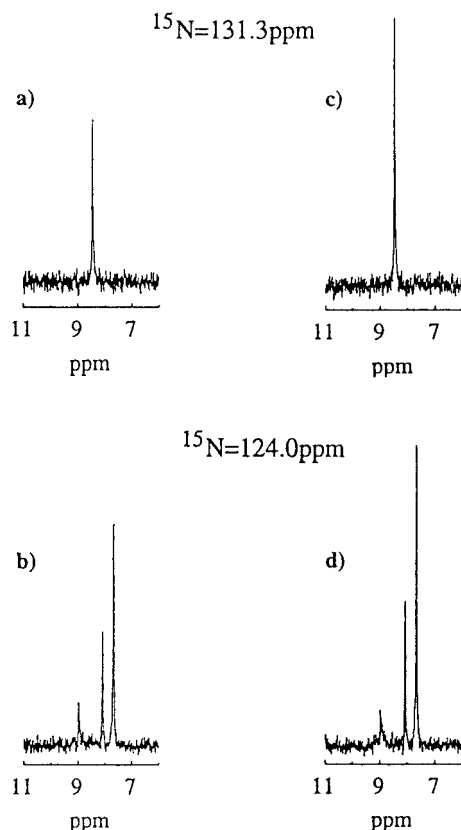


Figure 13 Cross section from ^1H - ^{15}N HMQC spectra of calmodulin recorded with different pulse sequence: (a,b) from the conventional HMQC; (c,d) from gradient-enhanced HMQC with sensitivity-enhancement (gs-HMQC). In all these experiments, broadband decoupling during acquisition period was accomplished by GARP-1 (35) decoupling sequence. A spectrum was obtained by using the same acquisition and processing parameters for each. The 1D-slice shown here was scaled to the same noise level for comparison (45).

obtained by processing the data by the STATES method (36).

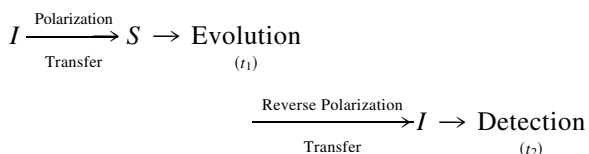
Figure 13 shows a cross section of the ^1H - ^{15}N HMQC spectra of calmodulin by different methods. Spectra were recorded on ^{15}N -labeled calmodulin at 30°C with a protein concentration of 1 mM at pH 6.8. The cross section of ^1H - ^{15}N HMQC spectra is scaled to the same noise level at ^{15}N chemical shifts 131.1 and 124.0 PPM. Figure 13(a,c) shows the cross section from the phase-cycled HMQC experiment (10) with water suppression achieved by a 70-Hz presaturation field for a duration of 1 sec. Figure 13(b,d) corresponds to the cross section from the gs-HMQC experiment. Suppression of the water signal is achieved by a pulsed-field gradient to avoid the sensitivity loss from exchangeable NH signals due to

presaturation. The gs-HMQC experiment achieves (45) sensitivity enhancement by factor of 1.43 ± 0.30 compared with a conventional HMQC experiment.

Thus a sensitivity-enhanced experiment, with or without gradients, has a signal-to-noise ratio that is greater by a factor of $\sqrt{2}$ than that of the phase-cycled experiment.

DIFFERENCES BETWEEN THE HMQC AND HSQC PULSE SEQUENCES

Both HMQC and HSQC sequences follow a similar polarization transfer strategy of the type given below:



However, there are several differences:

1. In HSQC sequence, the single quantum type: $2I_ZS_X$ or $2I_ZS_Y$ coherence exists during the evolution period, whereas, in the HMQC sequence, the coherence of the multiple-quantum type: $2I_XS_X$, $2I_XS_Y$ exists during evolution period.
2. In the HSQC sequence the Larmor precession of I -spin must be refocused in each delay τ separately (Fig. 5). In order to allow J modulation to proceed, this must be accomplished with nonselective 180° pulses. However, in the HMQC sequence (Fig. 6), one 180° pulse on I -spin refocuses the Larmor precession of I -spin during both delay periods τ .
3. In HSQC, characteristic T_2 relaxation time for antiphase SQ coherence ($2I_ZS_X$) is shorter than MQ coherence such as $2I_XS_Y$, which exists in the HMQC sequence. In principle this would allow higher resolution in the ω_1 dimension to the HMQC spectrum. In HSQC, the $2I_ZS_X$ term is not modulated by passive coupling (J_{HH}) of I -spin, whereas in HMQC the coherence $2I_XS_Y$ is modulated by passive coupling. HSQC yields singlets in the ω_1 dimension and HMQC yields multiplets (almost every proton in a molecule has at least some geminal or vicinal couplings to other protons), in practice the HSQC spectrum affords better resolution. Moreover, the collapse of multiplets into a singlet at least partly compensates for the intrinsically lower sensitivity of the HSQC sequence compared to

the HMQC sequence. In addition, if both I - and S -spins are subject to exchange broadening effects, the HMQC experiment suffers more, because both spins are in the xy plane.

4. For both phase-cycled and gradient-enhanced experiments, signal intensities are higher for multiple-quantum experiments, mainly because of the smaller number of RF pulses. This makes the HSQC sequence more sensitive to B_1 inhomogeneity. In practice, these experiments are usually incorporated as modules of more complex experiments and the choice of sequences depends on various factors such as convenience of incorporation and overall relaxation effects.

In many situations, the S -spin nucleus (e.g., ^{13}C) possesses multiple homonuclear (e.g., ^{13}C - ^{13}C) couplings, which manifest as splittings in the indirect (ω_1) dimension and effectively reduces resolution in that dimension. This problem can be circumvented in an important variation of the HSQC sequence known as the constant-time experiment.

CONSTANT TIME HSQC

The constant-time HSQC (CT-HSQC) experiment aims at eliminating the multiplet structure of the S -spin in the ω_1 dimension due to homonuclear couplings by using a constant-time ($2T$) period, during which t_1 evolution is combined with refocusing of homonuclear couplings (46–48).

The pulse sequence for CT-HSQC is shown in Fig. 14. For proteins, the effect of J -coupling between aliphatic and carbonyl carbons during t_1 is removed by a selective, off-resonance, 180° pulse on ^{13}CO . The second 180° pulse on ^{13}CO serves to refocus the phase twist experienced by the aliphatic ^{13}C nuclei due to Bloch-Siegert shift induced by off resonance decoupling pulse on ^{13}CO . Three observations between points (b,c) (Fig. 15) are to be noted. Chemical shift for the S -spin evolves for t_1 [$t_1/2 + T - (T - t_1/2) = t_1$] and heteronuclear coupling (J_{IS}) is decoupled [$t_1/2 - T + (T - t_1/2) = 0$]. However, homonuclear coupling (J_{CC}) evolves for the duration $2T$ time period [$-t_1/2 + T + T + t_1 = 2T$]. Magnetization at different points is described using the schemes given in the Appendix (Schemes III and IV).

$$(a \rightarrow b) \quad I_Z \xrightarrow{(90^\circ)I_X} -I_Y \xrightarrow{2J_{IS}t_2S_Z} -I_Y \cos 2\pi J_{IS}\tau + 2I_X S_Z \sin 2\pi J_{IS}\tau$$

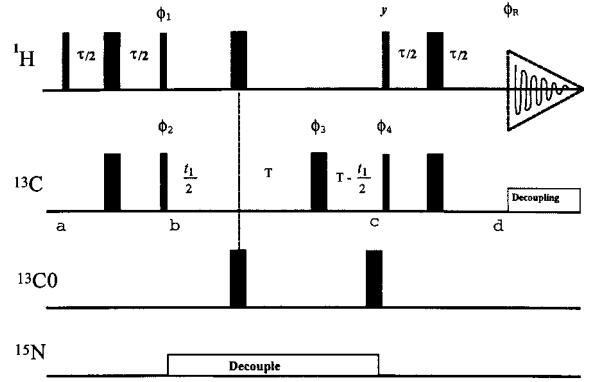


Figure 14 Pulse sequence for the ^1H - ^{13}C CT-HSQC experiment (41). Appropriate phase cycling is $\phi_1 = x, -x$; $\phi_2 = 8(x), 8(-x)$; $\phi_3 = 2(x), 2(y), 2(-x), 2(-y)$; $\phi_4 = 16(y), 16(-y)$; and receiver $\phi_R 2(x, -x, -x, x), 2(-x, x, x, -x)$. If required, this 32-step phase cycle may be reduced by a factor of 2 by eliminating cycling of ϕ_4 . The first and the last 180° (^{13}C) pulses are best applied as composite pulses of the type $90_x^\circ-180_y^\circ-180_x^\circ$, in order to minimize resonance offset and rf inhomogeneity effects. ^{15}N decoupling during the constant-time evolution period can be accomplished using a Waltz-16 (57) decoupling scheme, and ^{13}C decoupling during the data acquisition period can be accomplished with a GARP-1 (59) decoupling scheme. Net magnetization at different points (a–d) is described in the text.

$$\xrightarrow{\tau = 1/4J_{IS}} 2I_X S_Z \xrightarrow{(90^\circ)(I_Y + S_X)} -2I_Z S_Y$$

$$(b \rightarrow c) \xrightarrow{(\Omega_S)S_Z} -2I_Z S_Y \cos \Omega_S t_1 \cos^n(\pi J_{CC} 2T)$$

$$+ 2I_Z S_X \sin \Omega_S t_1 \cos^n(\pi J_{CC} 2T) + \text{antiphase terms}$$

The antiphase terms such as $4I_Z S_Y S_{2Z} \cos \Omega_S t_1 \sin^n(\pi J_{CC} 2T)$ and $8I_Z S_Y S_{2Z} S_{3Z} \sin \Omega_S t_1 \cos^n(\pi J_{CC} 2T)$ are not converted back to an observable proton magnetization by the reverse INEPT sequence following the constant-time evolution and can be ignored; n refers to the number of S -spin coupling partners. S_2, S_3 corresponds to other coupled ^{13}C nuclei. If the $2T$ time period is adjusted to n/J_{CC} , then $\cos^n(\pi J_{CC} 2T)$ gives negative or positive cross peaks for S -spins having an odd or even number of coupled partners, respectively:

$$(c \rightarrow d) \xrightarrow{(90^\circ)(I_Y + S_X)}$$

$$-2I_X S_Z \cos \Omega_S t_1 + 2I_X S_X \sin \Omega_S t_1$$

$$\xrightarrow[2J_{IS}I_Z S_Z]{\tau = 1/2J_{IS}} -I_Y \cos \Omega_S t_1 + 2I_X S_X \sin \Omega_S t_1 \quad [18]$$

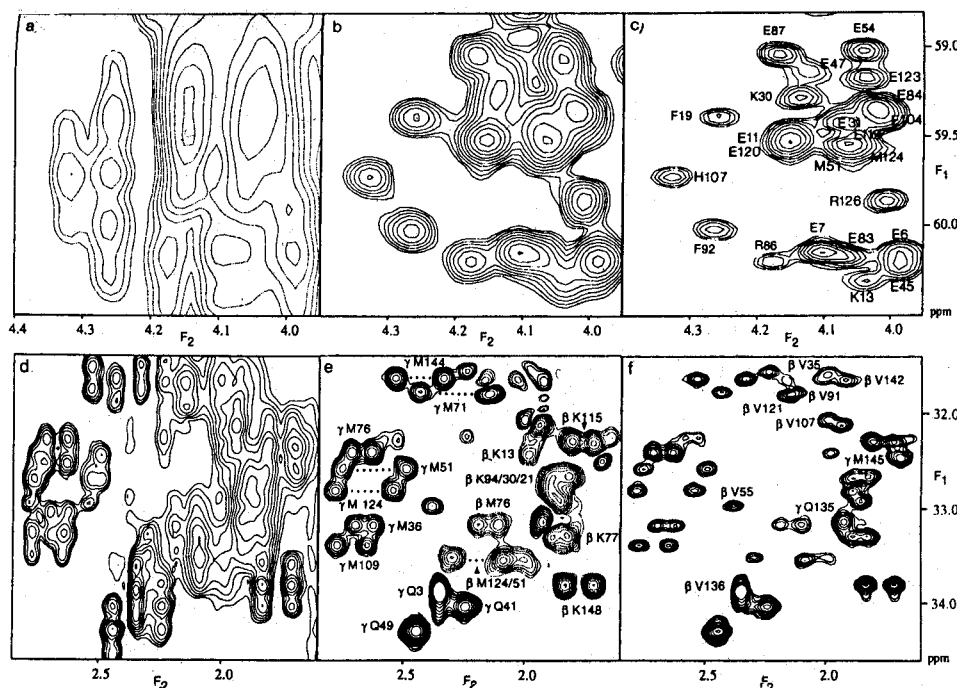


Figure 15 Comparison of the ^1H - ^{13}C shift correlation spectra (41) of the protein calmodulin recorded with (a,d) the regular HSQC experiment; (b,e) the CT-HSQC experiment with $2T = 26.6$ ms, and (c,f) the CT-HSQC experiment with $2T = 53.2$ ms. The spectral width in the ^{13}C dimension was adjusted to 5000 Hz (33 PPM) and the carrier was shifted postprocessing to 57 PPM. Therefore, resonance resonating upfield of 40.5 PPM appear at f_1 frequencies that are 33 PPM downfield from their actual chemical shift. For the CT-HSQC spectra, no phase correction was needed in the F_1 dimension, and negative contour levels correspond to carbons with an odd number of aliphatic carbon neighbors.

The resolution enhancement and spectral editing features of CT-HSQC are presented in Fig. 15. Generally ^{13}C - ^{13}C aliphatic coupling ranges from 32 to 40 Hz. The optimum length of $2T$ would be ≈ 27 ms to maximize the $\cos(\pi J_{\text{CC}} 2T)$ factor. Figure 15(a,b) refers to the conventional HSQC sequence as well as the CT-HSQC spectrum acquired with $2T = 54$ ms with identical resolution. Comparing the time domain signals of HSQC and CT-HSQC (5, 46, 49) and taking account of T_2 relaxation, one gets

$$F(t_1)_{\text{HSQC}} = \exp(-t_1/T_2) \exp(i\Omega_s t_1) \Pi \cos(\pi J_{\text{CC}} t_1) \quad [19]$$

$$F(t_1)_{\text{CT-HSQC}} = \exp(-2T/T_2) \exp(i\Omega_s t_1) \Pi \cos(\pi J_{\text{CC}} 2T) \quad [20]$$

The two major differences are the damping, $\exp(-t_1/T_2)$ in the HSQC sequence and $\exp(-2T/T_2)$ in CT-HSQC, and the J_{CC} modulates during t_1 in HSQC and during $2T$ in CT-HSQC. The absence of t_1 -dependent damping in CT-HSQC ensures no signal decay in the ω_1 dimension. The peaks in CT-HSQC are not split, but their intensity is diminished by a factor of

$\exp(-2T/T_2) \Pi \cos(\pi J_{\text{CC}} 2T)$. If T_2 is long enough and a suitable value of $2T$ selected so that $\Pi \cos(\pi J_{\text{CC}} 2T) \approx 1$, then the collapse of multiplets into singlets in CT-HSQC outweighs the intrinsic reduction in peak heights. An additional advantage of constant transverse relaxation is that the signal does not decay as a function of t_1 , and therefore, mirror image linear prediction is more efficient (50).

Finally, it should be noted that at natural abundance S - S couplings are of no consequence in the HSQC sequence, and therefore, the CT-HSQC experiment offers no advantage.

RECENT DEVELOPMENTS

In liquid-state NMR, spin relaxation due to cross-correlation of two anisotropic spin interactions can provide useful information about molecular structure and dynamics. These effects are manifested as differential line widths or line intensities in the NMR spectra. In the past, cross-correlation effects have been considered more of a nuisance than a benefit. Recently, it has become clear that cross-correlation ef-

fects can be utilized in order to decrease transverse relaxation rates and thus enable NMR spectroscopy of very large systems (51, 52). It has been recognized that at very high magnetic field strengths, cross correlation between dipole-dipole (DD) and chemical shift anisotropy (CSA) interactions in a ^{15}N - ^1H pair can be utilized to obtain sharp line widths for very large proteins. An important pulse sequence called TROSY (transverse relaxation optimized spectroscopy) has been developed based on cross-correlation phenomenon.

TROSY is basically a heteronuclear correlation experiment in which the proton magnetization is first transferred to ^{15}N (or ^{13}C) that evolves during t_1 [with differential relaxation rate of the ^{15}N doublet due to CSA (^{15}N)-dipole (^{15}N - ^1H) cross-correlation]. Magnetization is transferred back to the proton prior to detection [with differential line broadening of the proton doublet due to CSA (^1H)-dipole (^1H - ^{15}N) cross-correlation]. The resulting cross peak is a multiplet of four peaks, each having different widths, in the ω_1 and ω_2 dimensions. On the contrary, these four multiplets from each amide proton in the HSQC spectra averages to generate one peak due to application of 180° pulse on I -spin during t_1 evolution as well as ^{15}N decoupling during detection. In TROSY spectra, among these four multiplets, one which is not affected by line broadening due to $\text{DD} \times \text{CSA}$ cross-correlation is selected by the application of intuitive phase cycling. Details regarding TROSY are beyond the scope of this review and can be found elsewhere (53–56).

CONCLUSION

It has been the intention of the authors to describe a selection of fundamental experiments that are necessary for resonance assignments and structure determination of isotope-labeled proteins. The basic unifying features of pulse sequences have been presented so that the underlying mechanics of even complicated sequences become more transparent. In addition, the mathematical derivations have been given in great detail with the hope that this will help a newcomer to understand the latest pulse sequence techniques more easily.

ACKNOWLEDGMENTS

We thank Prof. Norbert Müller, Prof. O.W. Sørensen, Prof. R. Konrat, Drs. Michael Sattler, and R.J. McClure for suggestions. Academic Press (Figs. 4, 6–9,

and 13–15) and American Chemical Society (Figs. 5, 10, and 11) are acknowledged for giving permission to reproduce figures. Finally, thanks to Ms. Ratna Mandal for typing this manuscript.

APPENDIX

For a single spin, three angular momentum operations are needed for a complete description, i.e., I_x , I_y , and I_z . For two spins, an additional subscript, 1 or 2 is necessary to indicate which spin they refer to: Spin 1: $I_{1x}I_{1y}I_{1z}$, Spin 2: $I_{2x}I_{2y}I_{2z}$.

Scheme I: Commutator Relations

$$[I_z, I_z S_z] = [I_z, I_z] S_z = 0 \quad [\text{A1}]$$

$$[I_z S_z, I_z] = [I_z, I_z] S_z = 0 \quad [\text{A2}]$$

$$[I_x, I_y] = i I_z \quad [\text{A3}]$$

$$[I_y, I_z] = i I_x \quad [\text{A4}]$$

$$[I_z, I_x] = i I_y \quad [\text{A5}]$$

$$[S_x, S_y] = i S_z \quad [\text{A6}]$$

$$[S_y, S_z] = i S_x \quad [\text{A7}]$$

$$[S_z, S_x] = i S_y \quad [\text{A8}]$$

Scheme II: Coherence Space for Two-Spin System

Coherence	Coherence Name
I_z	Longitudinal I -spin
S_z	Longitudinal S -spin
I_x, S_y, I_y, S_x	Transverse I - and S -spin
$I_z S_z$	Longitudinal two-spin order
$I_x S_z, I_y S_z$	Transverse I -spin antiphase with S -spin
$I_z S_x, I_z S_y$	Transverse S -spin antiphase with I -spin
$I_x S_x, I_y S_x, I_x S_y, I_y S_y$	Multiple-quantum coherence

Scheme III: Free Precession

During the period of precession, the effect of chemical shift and scalar coupling evolution must be considered. For I -spin, the $\mathcal{H} = \Omega_I I_z$, where Ω_I is the

offset of the I -spin, and rotation during the delay τ can be presented as follows:

$$I_X \xrightarrow{(\Omega_I)I_Z} I_X \cos \Omega_I \tau + I_Y \sin \Omega_I \tau \quad [\text{A9}]$$

$$I_Y \xrightarrow{(\Omega_I)I_Z} I_Y \cos \Omega_I \tau - I_X \sin \Omega_I \tau \quad [\text{A10}]$$

$$I_Z \xrightarrow{(\Omega_I)I_Z} I_Z \quad [\text{A11}]$$

For two-spin systems (I and S) the form of Hamiltonian for spin-spin scalar coupling (J_{IS}) can be written as $\mathcal{H} = 2\pi J_{IS} I_Z S_Z$. The magnetization under spin-spin coupling is as follows:

$$I_X \xrightarrow{2J_{IS}I_Z S_Z} I_X \cos \pi J_{IS} \tau + 2I_Y S_Z \sin \pi J_{IS} \tau \quad [\text{A12}]$$

$$I_Y \xrightarrow{2J_{IS}I_Z S_Z} I_Y \cos \pi J_{IS} \tau - 2I_X S_Z \sin \pi J_{IS} \tau \quad [\text{A13}]$$

$$2I_Y S_Z \xrightarrow{2J_{IS}I_Z S_Z} 2I_Y S_Z \cos \pi J_{IS} \tau - I_X \sin \pi J_{IS} \tau \quad [\text{A14}]$$

$$2I_X S_Z \xrightarrow{2J_{IS}I_Z S_Z} 2I_X S_Z \cos \pi J_{IS} \tau + I_Y \sin \pi J_{IS} \tau \quad [\text{A15}]$$

$$2I_X S_X \xrightarrow{2J_{IS}I_Z S_Z} 2I_X S_X \quad [\text{A16}]$$

$$2I_X S_Y \xrightarrow{2J_{IS}I_Z S_Z} 2I_X S_Y \quad [\text{A17}]$$

$$2I_Y S_X \xrightarrow{2J_{IS}I_Z S_Z} 2I_Y S_X \quad [\text{A18}]$$

$$2I_Y S_Y \xrightarrow{2J_{IS}I_Z S_Z} 2I_Y S_Y \quad [\text{A19}]$$

Multiple quantum coherence does not evolve under spin-spin coupling.

General Rule for Rotation

$$I_\alpha \xrightarrow{(\theta)I_\beta} I_\alpha \cos \theta - i[I_\beta, I_\alpha] \sin \theta \quad \text{for } [I_\beta, I_\alpha] \neq 0 \quad [\text{A20}]$$

$$I_\alpha \xrightarrow{(\theta)I_\beta} I_\alpha \quad \text{for } [I_\beta, I_\alpha] = 0 \quad [\text{A21}]$$

where α, β are the possible combinations of x, y , and z axis.

Scheme IV: Effect of Radio Frequency Pulse

$$I_Z \xrightarrow{(90^\circ)I_Y} I_X \quad [\text{A22}]$$

$$I_X \xrightarrow{(90^\circ)I_X} I_X \quad [\text{A23}]$$

$$I_Z \xrightarrow{(90^\circ)I_X} -I_Y \quad [\text{A24}]$$

$$I_Y \xrightarrow{(90^\circ)I_X} I_Z \quad [\text{A25}]$$

$$I_Y \xrightarrow{(90^\circ)I_Y} I_Y \quad [\text{A26}]$$

$$2I_Y S_Z \xrightarrow{(90^\circ)S_X} -2I_Y S_Y \quad [\text{A27}]$$

Scheme V

Spin rotation in terms of raising and lowering operator. The coherence transfer formalism (15, 21) use shift operators, otherwise known as raising and lowering operators. These operators are related to the angular momentum operators by

$$I^+ = I_X + iI_Y \quad [\text{A28}]$$

$$I^- = I_X - iI_Y \quad [\text{A29}]$$

The effects of radio frequency pulses, chemical shift, and spin coupling on different coherence level are as follows:

$$2I_X S_X = 1/2(I^+ S^+ + I^- S^+ + I^+ S^- + I^- S^-)$$

$$2I_X S_Y = 1/2i(I^+ S^+ + I^- S^+ - I^+ S^- + I^- S^-)$$

$$2I_Y S_X = 1/2i(I^+ S^+ - I^- S^+ + I^+ S^- + I^- S^-)$$

$$2I_Y S_Y = -1/2(I^+ S^+ + I^+ S^- - I^- S^+ + I^- S^-)$$

Effect of Radio Frequency Pulse

$$I_Z \xrightarrow{(90^\circ)I_X} -i/2(I^- - I^+) \quad [\text{A30}]$$

$$I_Z \xrightarrow{(90^\circ)I_Y} 1/2(I^- + I^+) \quad [\text{A31}]$$

$$I^+ \xrightarrow{(90^\circ)I_x} 1/2(I^- + I^+) + iI_z \quad [\text{A32}]$$

$$I^+ \xrightarrow{(90^\circ)I_y} -1/2(I^- + I^+) + I_z \quad [\text{A33}]$$

$$I^- \xrightarrow{(90^\circ)I_x} 1/2(I^- + I^+) - iI_z \quad [\text{A34}]$$

$$I^- \xrightarrow{(90^\circ)I_y} 1/2(I^- + I^+) + I_z \quad [\text{A35}]$$

$$I^\pm \xrightarrow{(180^\circ)I_x} I^\mp \quad [\text{A36}]$$

$$I^\pm \xrightarrow{(180^\circ)I_y} -I^\mp \quad [\text{A37}]$$

Chemical Shift Effect

$$I^\pm \xrightarrow{(\Omega\tau)I_z} I^\pm e^{\pm i\Omega\tau} \quad [\text{A38}]$$

Spin Coupling Effect

$$I^+ \xrightarrow{(2J_{IS}I_zS_z\tau)} I^+ \cos(\pi J_{IS}\tau) - 2iS_z I^+ \sin(\pi J_{IS}\tau) \quad [\text{A39}]$$

$$I^- \xrightarrow{(2J_{IS}I_zS_z\tau)} I^- \cos(\pi J_{IS}\tau) + 2iS_z I^- \sin(\pi J_{IS}\tau) \quad [\text{A40}]$$

REFERENCES

1. Jeener J. 1971. Ampere summer school, Basko Polje, Yugoslavia; also in NMR and more in honour of Anatole Abragam, les editions de physiques 265–278.
2. Ernst R. 1975. Multidimension NMR. *Chimia* 29:179–187.
3. Bodenhausen G, Freeman R, Neidermeyer R, Turner D. 1977. Double Fourier transformation in high-resolution NMR. *J Magn Reson* 26:133–164.
4. Jeener J, Meier BH, Bachman P, Ernst R. 1979. Investigation of exchange processes by two-dimensional NMR spectroscopy. *J Chem Phys* 71:4546–4553.
5. Bax A, Freeman R. 1981. Investigation of complex networks of spin-spin coupling by two-dimensional NMR. *J Magn Reson* 44:542–561.
6. Maudsley A, Ernst R. 1977. Indirect detection of magnetic resonance by heteronuclear two-dimensional spectroscopy. *Chem Phys Lett* 50:368–372.
7. Ernst R, Bodenhausen G, Wokaun A. 1987. Principles of nuclear magnetic resonance in one and two dimensions. Oxford: Clarendon Press.
8. Bodenhausen G, Freeman R. 1977. Correlation of proton and carbon-13 NMR spectra by heteronuclear two-dimensional spectroscopy. *J Magn Reson* 28:471–474.
9. Bodenhausen G, Freeman R. 1978. Correlation of chemical shifts of protons and carbon-13. *J Am Chem Soc* 100:320–321.
10. Muller L. 1979. Sensitivity enhanced detection of weak nuclei using heteronuclear multiple quantum coherence. *J Am Chem Soc* 101:4481–4484.
11. Bax A, Griffey R, Hawkins B. 1983. Correlation of proton and nitrogen-15 chemical shifts by multiple quantum NMR. *J Magn Reson* 55:301–315.
12. Bodenhausen G, Ruben D. 1980. Natural abundance nitrogen-15 NMR by enhanced heteronuclear spectroscopy. *Chem Phys Lett* 69:185–189.
13. Bax A, Kay LE, Torchia D, Tschudin R. 1990. Comparison of different modes of two-dimensional reverse-correlation NMR for the study of proteins. *J Magn Reson* 86:304–318.
14. Norwood T, Boyd J, Heritage J, Soffe N, Campbell I. 1990. Comparison of techniques for 1H-detected heteronuclear 1H–15N spectroscopy. *J Magn Reson* 87:488–501.
15. Sørensen O, Eich G, Levitt M, Bodenhausen G, Ernst R. 1983. Product operator formalism for the description of NMR pulse experiments. *Prog NMR Spectroscopy* 16:163–192.
16. Van de Ven F, Hilbers C. 1983. Simple formalism for the description of multiple-pulse experiments, application to a weakly coupled two-spin($I=\frac{1}{2}$) system. *J Magn Reson* 54:512–520.
17. Van de Ven F. 1995. Multidimensional NMR in liquids. Basic principles and experimental methods. New York: VCH.
18. Slichter C. 1996. Principle of magnetic resonance. Berlin: Springer. p 1–456.
19. Hahn E, Maxwell D. 1952. Spin-echo measurement of nuclear spin-coupling in molecules. *Phys Rev* 88:1070–1084.
20. Carr HY, Purcell EM. 1954. Effects of diffusion on free precession in nuclear magnetic resonance experiments. *Phys Rev* 94:630–638.
21. Bain A. 1984. Coherence levels and coherence pathways in NMR. A simple way to design phase cycling procedures. *J Magn Reson* 56:418–427.
22. Bodenhausen G, Kogler H, Ernst R. 1984. Selection of coherence-transfer pathways in NMR pulse experiments. *J Magn Reson* 58:370–388.
23. Barker P, Freeman R. 1985. Pulsed field gradients in NMR. An alternative to phase cycling. *J Magn Reson* 64:334–338.
24. Hurd R. 1990. Gradient enhanced spectroscopy. *J Magn Reson* 87:3422–3428.
25. Vuister G, Kaptein R, Hurd R, John B, van Zijl P. 1991. Gradient-enhanced HMQC and HSQC spectroscopy. Applications to ^{15}N -labeled Mnt repressor. *J Am Chem Soc* 113:9688–9690.
26. Hurd R, John B. 1991. Gradient-enhanced proton-de-

- tected heteronuclear multiple quantum coherence spectroscopy. *J Magn Reson* 91:648–653.
27. Tolman J, Chung J, Prestegard J. 1992. Pure-phase heteronuclear multiple-quantum spectroscopy using field gradient selection. *J Magn Reson* 98:462–467.
 28. Grzesiek S, Bax A. 1993. The importance of not saturating H₂O in protein NMR. Application to sensitivity enhancement and NOE measurements. *J Am Chem Soc* 115:12593–12594.
 29. Li Y-C, Montelione G. 1993. Solvent saturation-transfer effects in pulsed-field-gradient heteronuclear single-quantum-coherence (PFG-HSQC) spectra of polypeptides and proteins. *J Magn Reson Series B* 101:315–319.
 30. Ruiz-Cabello J, Vuister G, Moonen C, Van Gelderen P, Cohen J, Van Zijl P. 1992. Gradient-enhanced heteronuclear correlation spectroscopy. Theory and experimental aspects. *J Mag Reson* 100:282–302.
 31. Boyd J, Soffe N, John B, Plant D, Hurd R. 1992. The generation of phase-sensitive 2D ¹⁴N-¹H spectra using gradient pulses for coherence-transfer-pathway selection. *J Magn Reson* 98:660–664.
 32. Bax A, Pochapsky SS. 1992. Optimized recording of heteronuclear multidimensional NMR spectra using pulse field gradients. *J Magn Reson* 99:638–643.
 33. Bendel P, Van Zijl P. 1994. Gradient enhanced proton-detected heteronuclear NMR at improved resolution. *J Magn Reson A* 110:130–135.
 34. Sattler M, Schleucher J, Griesinger C. 1999. Heteronuclear multidimensional NMR experiments for the structure determination of protein in solution employing pulse field gradient. *Prog Nuclear Magn Reson* 34:93–158.
 35. Davis A, Laue E, Keller J, Moskau D, Lohman J. 1991. Absorption-mode two-dimensional NMR spectra recorded using pulsed field gradients. *J Magn Reson* 94:637–644.
 36. States D, Haberkorn R, Ruben D. 1982. A two-dimensional nuclear overhauser experiment with pure absorption phase in four quadrants. *J Magn Reson* 48:286–292.
 37. Morris G, Freeman R. 1979. Enhancement of nuclear magnetic resonance signals by polarization transfer. *J Am Chem Soc* 101:760–762.
 38. Palmer IA, Cavanagh J, Wright P, Rance M. 1991. Sensitivity improvement in proton-detected two-dimensional heteronuclear correlation NMR spectroscopy. *J Magn Reson* 93:151–170.
 39. Cavanagh J, Palmer A, Wright P, Rance M. 1991. Sensitivity improvement in proton-detected two dimensional heteronuclear relay spectroscopy. *J Magn Reson* 91:429–436.
 40. Cavanagh J, Rance M. 1993. Sensitivity-enhanced NMR techniques for the study of biomolecules. *Annu Rep NMR Spect* 27:1–58.
 41. Vuister G, Cabello J, Van Zijl P. 1992. Gradient-enhanced multiple-quantum filter (Ge-MQF). A simple way to obtain single-scan phase-sensitive HMQC spectra. *J Magn Reson* 100:215–220.
 42. Altieri A, Miller K, Byrd R. 1996. A comparison of water suppression techniques using pulsed field gradients for high-resolution NMR of biomolecules. *Magn Res Rev* 17:27–82.
 43. Davis A, Keeler J, Laue E, Moskau D. 1992. Experiments for recording pure-absorption heteronuclear correlation spectra using pulsed field gradients. *J Magn Reson* 98:207–216.
 44. Kay L, Keifer P, Saarinen T. 1992. Pure absorption gradient enhanced heteronuclear single quantum correlation spectroscopy with improved sensitivity. *J Am Chem Soc* 114:10663–10665.
 45. Zhu G, Kong X, Sze K. 1998. Gradient- and sensitivity-enhanced heteronuclear multiple-quantum correlation spectroscopy. *J Magn Reson* 135:232–235.
 46. Vuister G, Bax A. 1992. Resolution enhancement and spectral editing of uniformly ¹³C-enriched proteins by homonuclear broadband ¹³C decoupling. *J Magn Reson* 98:428–435.
 47. Powers R, Gronenborn A, Clore G, Bax A. 1991. Three-dimensional triple-resonance NMR of ¹³C/¹⁵N-enriched proteins using constant time evolution. *J Magn Reson* 94:209–213.
 48. Santoro J, King G. 1992. A constant-time 2D Overhauser experiment for inverse correlation of isotopically enriched species. *J Magn Reson* 97:202–222.
 49. Marion D, Wüthrich K. 1983. Application of phase-sensitive two-dimensional correlated spectroscopy (COSY) for measurements of ¹H-¹H spin-spin coupling constants in proteins. *Biochem Biophys Res Commun* 113:967–974.
 50. Zhu G, Bax A. 1990. Improved linear prediction for truncated signals of known phase. *J Magn Reson* 90:405–410.
 51. Mandal PK, Madhu P, Muller N. 2000. Nuclear magnetic relaxation of methyl protons in a paramagnetic protein: cross-correlation effects. *Chem Phys Lett* 320:269–276.
 52. Boisbouvier J, Gans P, Blackledge M, Brutscher B, Marion D. 1999. Long-range structural information in NMR studies of paramagnetic molecules from electron spin-nuclear spin cross-correlated relaxation. *J Am Chem Soc* 121:7700–7701.
 53. Pervushin K, Riek R, Wider G, Wüthrich K. 1997. Transverse. Attenuated T2 relaxation by mutual cancellation of dipole-dipole coupling and chemical shift anisotropy indicates an avenue to NMR structures of very large biological macromolecules in solution. *Proc Natl Acad Sci USA* 94:12366–12371.
 54. Pervushin K. 2000. Impact of transverse relaxation-optimised spectroscopy (TROSY) on NMR as technique in structural biology. *Q Rev Biophys* 33:161–167.
 55. Cananagh J, Fairbrother W, Palmer A III, Skelton N. 1996. Protein NMR spectroscopy and principles and practice. New York: Academic Press.

56. Griesinger C, Schwalbe H, Schleucher J, Sattler M. 1994. Proton-detected heteronuclear and multidimensional NMR. In: Two-dimensional NMR spectroscopy: applications for chemists and biochemists. New York: VCH.
57. Shaka A, Keeler J, Freeman R. 1983. Evaluation of a new broadband decoupling scheme: WALTZ-16. *J Magn Reson* 53:313–340.
58. Levitt MH, Freeman R. 1979. NMR population inversion using composite pulse. *J Magn Reson* 33:473–476.
59. Shaka A, Barker P, Freeman R. 1985. Computer-optimized decoupling scheme for widespread application and low-level operation. *J Magn Reson* 64:547–552.

BIOGRAPHY



Pravat K. Mandal is a graduate from Indian Institute of Technology, Madras, where he studied for his doctorate under Prof. P.T. Manoharan. He joined as Visiting Scholar at University of California, Davis with Prof. G.N. Lamar. He worked briefly as Scientist in the Johannes Kepler University, Linz, Austria with Prof. Norbert Muller. Later he moved to the University of Pittsburgh Medical Center as Faculty member. His research interests focus on NMR studies on membrane protein and “Raft”-A β peptide interactions primarily in Alzheimer’s disease.